Marine Structures 33 (2013) 265–296

Contents lists available at ScienceDirect

Marine Structures

journal homepage: www.elsevier.com/locate/marstruc

A simplified analytical method for estimating the crushing resistance of an inclined ship side

Loïc Buldgen [a,*,1], Hervé Le Sourne [b], Philippe Rigo [a]

[a] University of Liège, ANAST, 1 Chemin des Chevreuils, 4000 Liège, Belgium
[b] ICAM Nantes, 35 Avenue du champ de Manœuvres, 44470 Carquefou, France

ARTICLE INFO

Article history:
Received 3 April 2013
Received in revised form 27 May 2013
Accepted 29 June 2013

Keywords:
Ship collision
Analytical formulation
Super-elements method
Crashworthiness
Inclined plate

ABSTRACT

This paper provides a new contribution to the simplified analytical treatment of collisions between two ships. It is directly connected to the well-known super-elements method, which is a simplified procedure allowing for a quick estimation of the damages caused to both the striking and struck vessels during such events. In this article, a new analytical formulation is presented for estimating the impact resistance provided by inclined ship side panels. Two different scenarios are treated. We first deal with the case of an impact between the oblique plate and the stem of the striking ship, and then we consider the situation where the inclined panel is impacted by the bulb. For these two scenarios, an analytical formulation relating the force and the penetration is provided and these developments are validated by comparing them to the results of finite elements simulations. Finally, the new inclined plate super-element is integrated in a simplified model of a frigate collided by another ship, and the resistance given by the super-elements method is then compared to the one obtained by a numerical simulation of this collision.

* *Corresponding author.* Tel.: +32 (0) 4 366 48 59/+32 (0) 478 50 21 88 (mobile); fax: +32 (0) 4 366 91 33.
E-mail addresses: L.Buldgen@ulg.ac.be, L.Buldgen@ulg.ac.be (L. Buldgen), herve.lesourne@icam.fr (H. Le Sourne), ph.rigo@ulg.ac.be (P. Rigo).
[1] FRIA PhD Student.

0951-8339/$ – see front matter © 2013 Elsevier Ltd. All rights reserved.
http://dx.doi.org/10.1016/j.marstruc.2013.06.005

1. Introduction

Many different loads have to be considered when designing a new vessel. Amongst them, the collision with another ship has to be treated carefully, in particular for military applications or for the transport of polluting substances. To assess the impact resistance, it is of course possible to resort to finite elements simulations, where both the struck and striking vessels have to be represented. However, doing so is often time-expensive, as a realistic modeling of the complete collision process often requires very huge computing efforts. Sometimes, such an approach is not justified, in particular at the beginning of the design process, where the final structure of the vessel is not completely fixed. Moreover, if a kind of optimization process is followed to get the optimal shape for the ship, performing a great number of numerical simulations to re-evaluate each time the impact resistance is not realistic. For these reasons, engineers are more and more demanding for simplified design tools that may rapidly assess the ability of a vessel to withstand a collision. Minorsky [1] was the first to propose a fast empirical approach and since his pioneer work, many other investigations have led to very concluding results, as summarized by Pedersen [2].

A basic idea to get a simplified evaluation of the impact resistance is to divide the vessel into large structural entities. This approach was called the *idealized structural unit method* (ISUM) by Ueda and Rashed [3] who applied it successfully to the study of various ships. In the particular frame of collisions, a similar procedure called the *super-elements method* (SEM) was established by Lützen, Simonsen and Pedersen [4]. More recently, this application was associated by Le Sourne [5] to a rigid body movement analysis tool in order to consider both the internal and external mechanics during the collision process.

The present paper is a direct contribution to the super-elements method. In this approach, the vessel is decomposed into macro-components (such as girders, frames, stiffeners, plates…) called "super-elements". Each of them is characterized by an analytical law relating the indentation of the striking vessel to the crushing resistance provided by the component itself. The total impact force is then simply obtained by adding all these contributions and therefore, one of the most important steps is to coherently derive these individual crushing resisting forces for the various components.

In this article, we will focus on the particular case of the plating when it is submitted to a large impact load. Amongst others, this topic has already been investigated in details by Jones [6], Zhang [7] or Wang [8] and [9], but without accounting for:

- the inclination of the side shell plating: most of the publications available in the literature are only devoted to the case of vertical panels, but it is clear that all ships may not be represented only by such components.
- the shape of the impactor: the deformations of the side shell panels may be strongly influenced by the striking profile. In particular, one has to distinguish between the case of an impact involving the stem or the bulb of the ship, because the form of these two elements is strongly different.

Consequently, this paper aims to provide an innovative contribution to the super-elements method by deriving new closed-form expressions characterizing the resistance of an inclined side panel to collisions involving the bulb or the stem of the striking vessel. For these two cases, an analytical procedure based on the upper-bound method is followed to get a mathematical equation relating the impact force to the penetration of the colliding ship. This law is then validated by comparisons with numerical results obtained through finite elements simulations using the non-linear code LS-DYNA. Finally, to get a global validation, a collision is simulated on a simplified model representing a frigate at rest.

2. Geometrical description of the problem

In order to give an overall view of the problem, it is first necessary to describe precisely all the geometrical parameters defining the *plate*, the *bulb* and the *stem*, that are potentially required to fix the collision process.

The *plate* is geometrically characterized by its lengths a and b, its inclination angle α and its thickness t_p (see Fig. 1). A local reference frame (x, y, z) is defined in its plane, in such a way that x and y

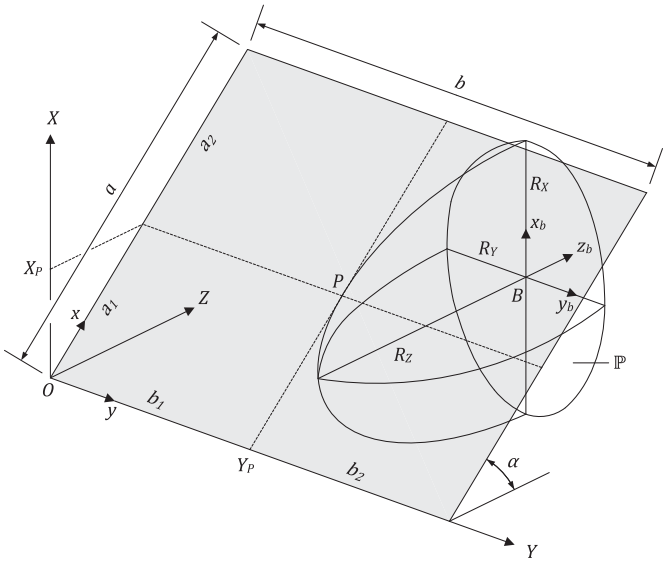

Fig. 1. Collision between the bulb and the inclined plate.

are respectively oriented along the inclined and horizontal side of the plate (see Fig. 1). The origin O of (x, y, z) is the left lowermost corner of the plate.

2.1. Impact by a bulb

The shape of the *bulb* of the striking vessel is idealized as an elliptic paraboloid $\mathbb{P}$, whose centre is denoted by B (see Fig. 1). This point remains fixed in space, which means that B is not following the bulb during the collision process. Considering a local reference frame (x_b, y_b, z_b) attached to point B, the equation of the closed volume Ω_b limiting the bulb may be written as:

$$\Omega_b \equiv \frac{x_b^2}{R_X^2} + \frac{y_b^2}{R_Y^2} \leq \frac{z_b + R_Z + \delta}{R_Z} \tag{1}$$

with $z_b \leq -\delta$. In Eq. (1), δ is the current penetration of the striking ship and R_X, R_Y, R_Z are the three radii characterizing the paraboloid $\mathbb{P}$ along the axes x_b, y_b, z_b respectively. The first contact between the bulb and the shell plating occurs at point P, where a tangency condition is simply achieved. In the global coordinate system (X, Y, Z) attached to point O, P is defined by its three coordinates (X_P, Y_P, Z_P) that can be found only by geometrical considerations. The definition of X_P and Y_P allows then for a spatial partition of the plate, which may be divided in four regions as depicted in Fig. 1, with:

$$a_1 = X_P/\sin\alpha, \quad a_2 = a - a_1, \quad b_1 = Y_P, \quad b_2 = b - b_1 \tag{2}$$

2.2. Impact by the stem

The stem of the striking vessel is assumed to be bounded by an external surface assimilated to a paraboloid $\mathbb{P}$ with variable radii (see Fig. 2). As a consequence, the shape of the uppermost deck is a parabola, whose center is a non-moving point S. This point is also the origin of a fixed local reference frame (x_s, y_s, z_s). In the uppermost deck, the two radii of the paraboloid $\mathbb{P}$ are denoted by p and q and they are progressively decreasing along the vertical x_s axis to reach the value of $p - h_b\cot\varphi$ and $q - h_b\cot\psi$ in the lowermost deck. The two angles φ and ψ are respectively called the stem and side

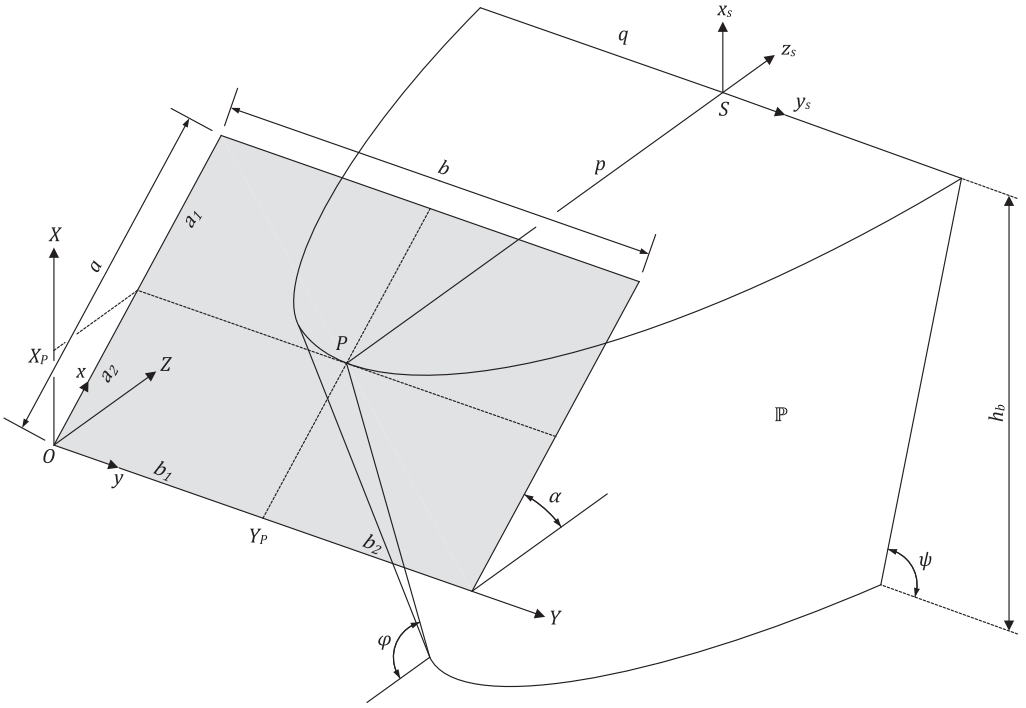

Fig. 2. Collision between the stem and the inclined plate.

angles, while h_b is simply the depth of the striking ship (see Fig. 2). According to all the previous definitions, the mathematical expression of the closed volume Ω_s limiting the bulb is:

$$\Omega_s \equiv \left(\frac{y_s^2}{(q + x_s \cot \psi)^2} - 1 \right) (p + x_s \cot \varphi) \leq z_s + \delta \tag{3}$$

with $z_s \leq -\delta$ and $-h_b \leq x_s \leq 0$. The first contact point P, characterized by its coordinates (X_P, Y_P, Z_P) in the global frame, is simply defined as the intersection of the uppermost deck with the plate, as depicted in Fig. 2.

The final shape of the striking bow, simply defined as the union of the two volumes Ω_b and Ω_s. Doing so leads to the configurations depicted in Fig. 3. Note that the two local coordinate systems (x_s, y_s, z_s) and (x_b, y_b, z_b) have been previously introduced to give an analytical expression of Ω_b and Ω_s, but it is clear that only the global system (X, Y, Z) may be used to characterize the relative position of the ship with respect to the plate.

Let us finally mention that the calculations detailed in this paper are only applicable to the case of an impact involving the bulb (see Fig. 4a) or the stem (see Fig. 4b). In other words, the scenario of a collision where both the bulb and the stem are simultaneously concerned (see Fig. 4c) is not treated here.

3. Collision scenario involving the stem

3.1. Definition of the displacements field

In this collision scenario, the needed geometrical data are the dimensions a, b, t_p of the plate, the inclination angle α and all the parameters h_b, p, q, ψ, φ characterizing the stem. Moreover, the horizontal

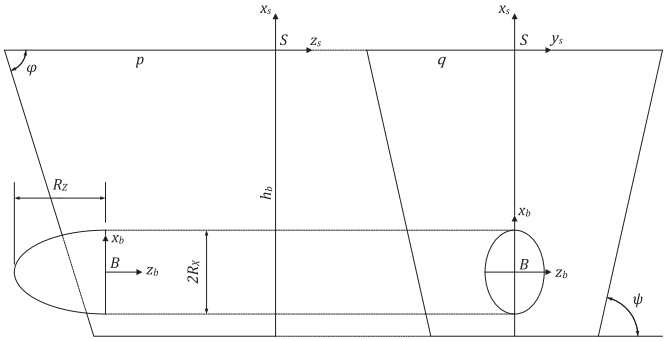

Fig. 3. Final configuration of the striking bow.

and vertical positions X_P and Y_P of the striking vessel are supposed to be known for defining the values a_1, a_2, b_1 and b_2. To evaluate the resistance provided by the plate during the impact, let's try to give a mathematical description of the displacements field $w(x, y)$ characterizing the deformation of the structure. Firstly, it is worth noticing that $w(x, y)$, defined in the local reference frame (x, y, z) of the plate (see Fig. 2), refers only to displacements perpendicular to the plane of the structure (see Fig. 5) only. We assume here that there is no motion in the (x, y) plane, which implies that the fibers constituting the plate are only submitted to an axial straining coming from an out-of-plane motion. This assumption implies that the potential friction between the ship and the structure is neglected.

As three dimensional representation of $w(x, y)$ is shown in Fig. 1 and it can be seen that the structure is forced to follow the shape of the stem in the horizontal plane $X = X_P$. In any plane perpendicular to the Y axis, the displacement is assumed to be simply linear. As a consequence, $w(x, y)$ may take the following form:

$$w(x, y) = W(y)f(x) \tag{4}$$

where $W(y)$ denotes the amplitude of the displacements in the horizontal plane $X = X_P$ and $f(x)$ is an interpolation function. $W(y)$ and $f(x)$ depend on δ and are defined hereafter.

Let's first consider the function $W(y)$, which represents the displacements parallel to the Z axis appearing in the horizontal plane $X = X_P$ (see Fig. 5). As shown in Fig. 6, $W(y)$ may be divided into three different parts $W_1(y)$, $W_2(y)$ and $W_3(y)$:

- For $y_1 \leq y \leq y_2$, the plate is forced to follow the displacements imposed by the stem, so $W_2(y)$ has to be defined in accordance with the parabolic shape of the uppermost deck.

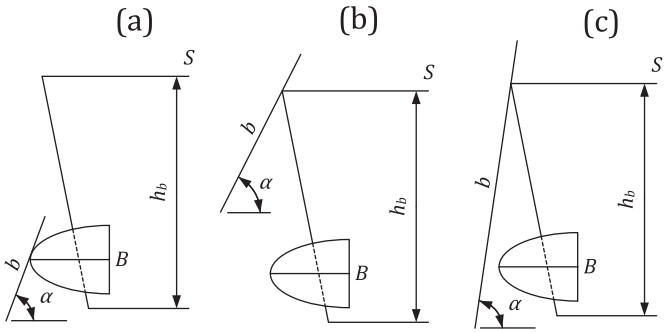

Fig. 4. Collisions scenario.

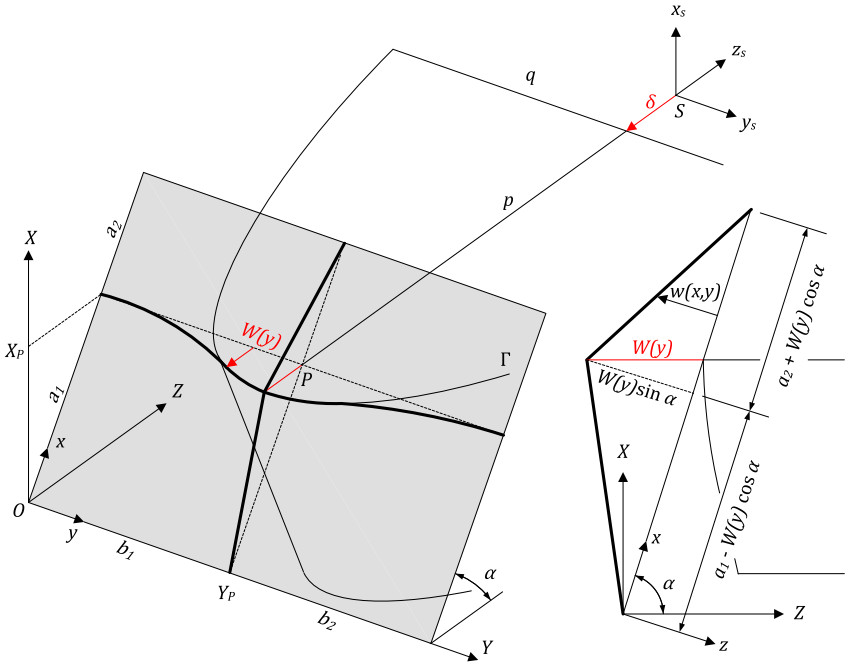

Fig. 5. Deformation pattern of an inclined plate impacted by the stem.

- For $0 \leq y \leq y_1$, the displacements have to respect the support conditions $W_1 = 0$ and $\partial W_1/\partial y = 0$ for $y = 0$ but also compatibility conditions for $y = y_1$. At this point, displacements and slopes have to verify $W_1 = W_2$ and $\partial W_1/\partial y = \partial W_2/\partial y$ an, as a consequence, it is clear that W_1 has to be a quadratic expression of y.
- For $y_2 \leq y \leq b$, the previous conditions have also to be imposed. So $W_3(y)$ has to satisfy $W_3 = 0$ and $\partial W_3/\partial y = 0$ for $y = b$, while W_2 and W_3 have to verify the conditions $W_2 = W_3$ and $\partial W_2/\partial y = \partial W_3/\partial y$ for $y = y_2$. So W_3 is then also a quadratic expression of y.

Even if the impact is not symmetric, it is clear that the displacements field chosen for the region $Y_P \leq y \leq b$ must be similar to the one on the section $0 \leq y \leq Y_P$. Therefore, in order to avoid any redundancy, our description will be limited to the first zone only. As mentioned earlier, the shape of the uppermost deck is a parabola described by the curve called Γ in Figs. 5 and 6. For $x_s = 0$, Eq. (3) defining Ω_s gives the equation of Γ. in the local (x_s, y_s, z_s) reference frame. However, knowing the precise initial location of point P, the equation of Γ in the global frame (X, Y, Z) is simply:

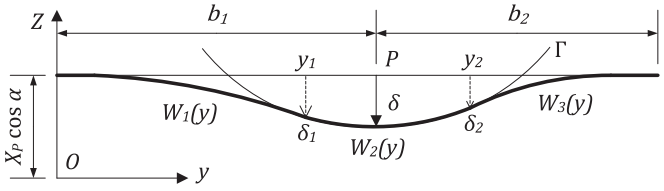

Fig. 6. Displacements profile in the horizontal plane $X = X_P$.

$$\Gamma \equiv Z - X_P \cos\alpha = \frac{p(y-Y_P)^2}{q^2} - \delta \rightarrow W_2(y) = \delta - \frac{p(y-b_1)^2}{q^2} \tag{5}$$

with $y_1 < y \leq b_1$. From (5), it is worth noting that $W_2 = \delta$ and $\partial W_2/\partial y = 0$ for $y = Y_P = b_1$, which is coherent with all the hypotheses considered so far. If we now consider the remaining region $0 \leq y \leq y_1$, accounting for all the compatibility conditions expressed here above, the quadratic expression of $W_1(y)$ is found to be:

$$W_1(y) = \delta_1 \frac{y^2}{y_1^2} \tag{6}$$

where δ_1 is the displacement for $y = y_1$. As shown by Eq. (6), the parameters δ_1 and y_1 still have to be defined to get a complete definition of $W(y)$. As explained earlier, they may be found by respecting the slope and displacement continuity for $y = y_1$, i.e.:

$$\begin{aligned} W_1 = W_2 = \delta_1 \Leftrightarrow \delta_1 &= \delta - \tfrac{p(y_1-b_1)^2}{q^2} \\ \tfrac{\partial W_1}{\partial y} = \tfrac{\partial W_2}{\partial y} \Leftrightarrow \tfrac{2\delta_1}{y_1} &= -\tfrac{2p(y_1-b_1)}{q^2} \end{aligned} \Leftrightarrow y_1 = b_1 - \frac{q^2}{p}\frac{\delta}{b_1}\,; \quad \delta_1 = \delta - \frac{q^2}{p}\frac{\delta^2}{b_1^2} \tag{7}$$

Note that y_1 and δ_1 are varying with the penetration. As expected, y_1 is decreasing with δ, while δ_1 is of course increasing with δ.

The characterization of the interpolation function $f(x)$ is much easier to achieve. To do so, let us consider the right part of Fig. 5, which shows the displacements profile in a plane perpendicular to the y axis. The maximal value of $w(x, y)$ is $W(y)\sin\alpha$ and is reached for $x = a_1 - W(y)\cos\alpha$. On the contrary, $w(x, y)$ has to be set to 0 for $x = 0$ and $x = a_1 + a_2$ because of the support conditions. Therefore, one can simply consider that $f(x)$ is defined by:

$$\begin{aligned} f_1(x) &= \tfrac{x\sin\alpha}{a_1 - W(y)\cos\alpha}, \quad \text{for } 0 \leq x \leq a_1 - W(y)\cos\alpha \\ f_2(x) &= \tfrac{(a_1+a_2-x)\sin\alpha}{a_2 + W(y)\cos\alpha}, \quad \text{for } a_1 - W(y)\cos\alpha < x \leq a_1 + a_2 \end{aligned} \tag{8}$$

As a conclusion, the displacements field $w(x, y)$ is entirely defined by Eqs. (5), (6) and (8), with the additional definitions given in (7). A summary is also provided by Table 1.

3.2. Derivation of the resistance

The resistance provided by the struck structure during the impact may now be evaluated by applying the upper-bound theorem (see Ref. [6] for more information). To do so, let us denote by F the total force exerted by the ship to impose an indentation δ and let us call E_{ext} the corresponding external work. According to the previous section, applying an indentation δ to the plate leads to the assumed displacements field $w(x, y)$ described above. Let us then call E_{int} the corresponding amount of energy dissipated internally by the plate. Provided that $w(x, y)$ is kinematically admissible, the upper-bound theorem states that equating the external work rate to the internal energy rate leads to an evaluation by excess of the resistance F. In other words, on may consider that the following equation:

$$\dot{E}_{ext} = \dot{E}_{int} \tag{9}$$

Table 1
Combination of $f(x)$ and $W(y)$ to get the total field $w(x, y)$.

	$0 \leq y \leq y_1$	$y_1 < y \leq b_1$	$b_1 < y \leq y_2$	$y_2 < y \leq b$
$[a_1 - W(y)\cos\alpha;\ a]$	$f_2(x)\cdot W_1(y)$	$f_2(x)\cdot W_2(y)$	$f_2(x)\cdot W_2(y)$	$f_2(x)\cdot W_3(y)$
$[0;\ a_1 - W(y)\cos\alpha]$	$f_1(x)\cdot W_1(y)$	$f_1(x)\cdot W_2(y)$	$f_1(x)\cdot W_2(y)$	$f_1(x)\cdot W_3(y)$

where the dot $(\cdot)$ denotes a time derivative, may give a good approximation of the resistance F, provided that $w(x, y)$ is chosen in a realistic way. Concerning this last point, it has to be noted that $w(x, y)$ is not strictly admissible, because of the slope discontinuity appearing along the line $x = a_1$ in Fig. 5. As a consequence, this line has to be considered as a plastic hinge, which causes a first part of the energy to be dissipated there. However, as the plate thickness is quite small, this phenomenon will be disregarded in the present paper.

In fact, the main part of the internal dissipation is coming from membrane effects taking place into the plate. These ones are much larger than the bending effects mentioned previously, which is an additional reason for neglecting the plastic hinge in $x = a_1$. So if we neglect bending, according to Zhang [7], the internal plastic energy rate is given by:

$$\dot{E}_{\text{int}} = \frac{2\sigma_0 t_p}{\sqrt{3}} \int_0^a \mathrm{d}x \int_0^b \sqrt{\dot{\varepsilon}_{xx}^2 + \dot{\varepsilon}_{yy}^2 + \dot{\varepsilon}_{xy}^2 + \dot{\varepsilon}_{xx}\dot{\varepsilon}_{yy}}\, \mathrm{d}y \tag{10}$$

where $\dot{\varepsilon}_{ij}$ is the strain rate tensor in the axes (x, y) and σ_0 is the flow stress of the material constituting the plate. The strain rates are related to the displacements $w(x, y)$ by the Green's definitions:

$$\dot{\varepsilon}_{xx} = \dot{\delta}\frac{\partial w}{\partial x}\cdot\frac{\partial^2 w}{\partial x \partial \delta}, \quad \dot{\varepsilon}_{yy} = \dot{\delta}\frac{\partial w}{\partial x}\cdot\frac{\partial^2 w}{\partial \delta \partial x}, \quad \dot{\varepsilon}_{xy} = \frac{\dot{\delta}}{2}\left(\frac{\partial w}{\partial x}\cdot\frac{\partial^2 w}{\partial \delta \partial y} + \frac{\partial w}{\partial y}\cdot\frac{\partial^2 w}{\partial \delta \partial x}\right) \tag{11}$$

where $w(x, y)$ is defined in accordance with Table 1. In theory, the previous relations have to be introduced in Eq. (10) to get the internal energy rate. Unfortunately, as the definitions of $w(x, y)$ are complex, it is practically impossible to get a closed-form expression for $\dot{E}_{\text{int}}$, and therefore and additional simplification has to be introduced. This one consists in neglecting the dissipation rate $\dot{\varepsilon}_{xy}$ due to shear, which is equivalent to admit that the plate is made of fibers oriented along the x and y directions submitted to independent axial deformations ε_{xx} and ε_{yy}. This plate strip formulation is also considered by Wierzbicki [10] for a punctual impact and is shown to be more conservative than evaluating $\dot{E}_{\text{int}}$ by including the shear strain energy. Following this assumption, Eq. (10) may be replaced by:

$$\dot{E}_{\text{int}} = \sigma_0 t_p \int_0^d \mathrm{d}x \int_0^b (\dot{\varepsilon}_{xx} + \dot{\varepsilon}_{yy})\mathrm{d}y = \dot{E}_x + \dot{E}_y \tag{12}$$

where $\dot{E}_x$ and $\dot{E}_y$ are respectively the energy rate associated to the fibers oriented along the x and y directions. In fact, as the displacements field $w(x, y)$ is different over the eight sub-areas dividing the initial surface $[a, b]$ of the plate (see Table 1), the previous integral (12) may be calculated by considering the individual contributions $\dot{E}_{x,i}$ and $\dot{E}_{y,i}$ coming from these eight regions, i.e.:

$$\dot{E}_{\text{int}} = \dot{E}_x + \dot{E}_y = \sum_{i=1}^{8} \dot{E}_{x,i} + \sum_{i=1}^{8} \dot{E}_{y,i} \tag{13}$$

where the first and (resp. second) summation term corresponds to the addition of the 8 individual energy rates of the fibers oriented along the x (resp. y) direction for the eight sub-surfaces in Table 1. Even if this last expression is simpler, the analytical derivation of $\dot{E}_{\text{int}}$ is however quite long. For this reason, the complete calculation is not detailed here but some indications are available in Appendix 1 for evaluating $\dot{E}_{x,i}$ and $\dot{E}_{y,i}$ on the eight regions. If we assume that the external work rate is simply given by $\dot{E}_{\text{ext}} = F\dot{\delta}$, applying (9) and considering (12) leads finally to the following formula for the resistance:

$$F = \sigma_0 t_p \int_0^a \mathrm{d}x \int_0^b \left(\frac{\partial w}{\partial x}\cdot\frac{\partial^2 w}{\partial x \partial \delta} + \frac{\partial w}{\partial x}\cdot\frac{\partial^2 w}{\partial \delta \partial x}\right) \mathrm{d}y = \sum_{i=1}^{8}\left(\frac{\dot{E}_{x,i}}{\dot{\delta}} + \frac{\dot{E}_{y,i}}{\dot{\delta}}\right) \tag{14}$$

3.3. Numerical validation

In order to validate the analytical developments presented here above and detailed in Appendix 1, some numerical simulations were performed by using the finite elements software LS-DYNA. This has

already been done in a previous communication of Buldgen et al. [11], where some results are given for a plate and a ship with other dimensions than those considered here. The comparisons performed hereafter are in fact an additional validation, as the geometrical properties characterizing the ship and the plate (see Table 2) varies from those given in Ref. [11]. It has to be mentioned here that the goal of the present section is only to validate the theoretical developments leading to the resistance F. Therefore, the plate dimensions given in Table 2 may not be consistent with the current practice in naval architecture.

The material is numerically defined as to reproduce the properties of mild steel. Its behavior is first characterized by a linear elastic phase defined by the Young modulus E. Once the yield stress σ_0 is reached, a linear plastic hardening phase defined by the tangent modulus E_T is assumed. The properties of the material are also given in Table 2.

The inclination of the plate defined by the angle α is varied from 0° (horizontal plate) to 90° (vertical plate). The results obtained for three different cases are plotted in Figs. 7–9.

As shown on these figures, the agreement between the analytical and the numerical results is quite satisfactory. This is also the case for other intermediate values of α, for which the results have not been reproduced in the present paper. Nevertheless, for the case of $\alpha = 90°$, the discrepancy between the numerical and analytical curves is quite important for large values of δ The divergence comes from the use of a non-hardening material in the theoretical approach, which is undoubtedly required for deriving a closed-form expression of F. As a matter of comparison, numerical simulations were also performed by imposing a zero tangent modulus E_T. Doing this leads to the curve called "Numerical, no hardening" in Fig. 9 that shows a much better agreement with the analytical prevision.

On Figs. 7–9, a comparison is also made with other analytical expressions already available in the literature. Zhang [7] derived a closed-form expression by assuming a punctual impact. The shape of the stem is therefore not taken into consideration in his developments. As expected, doing so leads to a little overestimation of the resistance for small values of δ, but the discrepancy is growing with the indentation. In fact, accounting for the shape of the striking bow allows for a better approximation of the curvature of $F(\delta)$. For this reason, the expression exposed in Ref. [7] and recalled in Appendix 1 by Eq. (57) appears to be over-conservative for large values of δ. For the particular case of a horizontal plate ($\alpha = 0°$), Simonsen [12] proposed the solution given by Eq. (58) in Appendix 1. As shown in Fig. 7, the agreement with our developments is satisfactory.

4. Collision involving the bulb

In this scenario, it is clear that the displacement pattern should be defined so as to be tangent to the elliptic paraboloid $\mathbb{P}$ (see Fig. 1) idealizing the assumed shape of the bulb. However, with such an approach, it is rather impossible to provide an analytical treatment of the problem. For this reason, the displacements field is simplified by considering the two solutions exposed in Fig. 10 (note that for the sake of clarity, only one half on the deformation pattern is depicted in Fig. 10, but the situation is of course similar for the remaining part of the plate):

- Solution 1 (see Fig. 10a): in this first approach, the displacements field accounts for the real shape of the bulb in the vertical plane π_1 defined by $Y = Y_P$. In this plane, the displacements are described by two curves Γ_1 and Γ_2 following the shape of the paraboloid $\mathbb{P}$ and respecting the support conditions in $x = 0$ and $x = a$. These displacements are then linearly interpolated along the straight

Table 2
Geometrical data used for numerical validations with LS-DYNA.

Properties of the plate			Properties of the stem			Properties of the material		
x Dimension	a	3 m	y Radius	q	1.5 m	Young modulus	E	210 GPa
y Dimension	b	2 m	z Radius	p	2.5 m	Yield stress	σ_0	240 MPa
Thickness	t_p	0.02 m	Height	h_b	2.5 m	Tangent modulus	E_T	1015 MPa
			Stem angle	φ	70°			
			Side angle	ψ	74°			

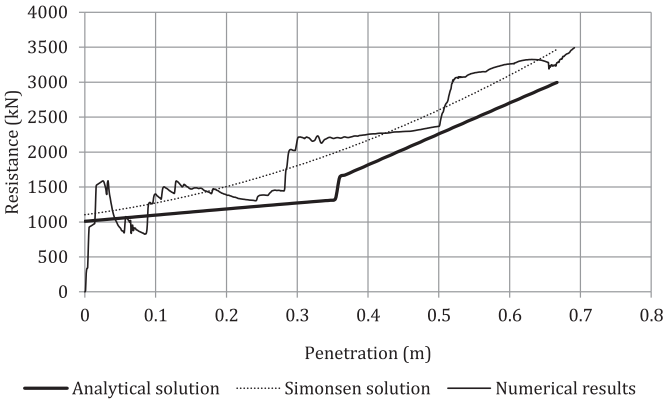

Fig. 7. Comparison between analytical and numerical results for $\alpha = 0°$.

lines Γ_3 and Γ_4 (Γ_4 is not depicted in Fig. 10a), so as to satisfy the support conditions in $y = 0$ and $y = b$.

- Solution 2 (see Fig. 10b): in this second approach, the displacements field accounts for the real shape of the bulb in the horizontal plane π_2 located in $X = X_P$. To do so, the curves Γ_3 and Γ_4 (Γ_4 is not depicted in Fig. 10b) are tangent to the paraboloid $\mathbb{P}$ and respects the support conditions in $y = 0$ and $y = b$. The displacements in the plane π_2 are then linearly interpolated along the straight lines Γ_1 and Γ_2 to also verify the support conditions in $x = 0$ and $x = a$.

So the present analytical treatment requires the development of two different solutions, depending on the necessity to respect the shape of the bulb in the vertical plane π_1 or in the horizontal one π_2. However, if we carefully analyze the situation depicted in Fig. 10b for solution 2, it may be noticed that the problem is mathematically identical to the one considered for the case of an impact involving the stem. This may be justify by the fact that the curve Γ corresponding to the intersection between the elliptic paraboloid $\mathbb{P}$ and the horizontal plane π_2 is itself a parabola of radii R_y and R_z. For this reason, all the developments performed in Section 3 remain valid, provided that the radii p and q defining the uppermost deck of the stem have to be replaced respectively by R_z and R_y. These two parameters are to

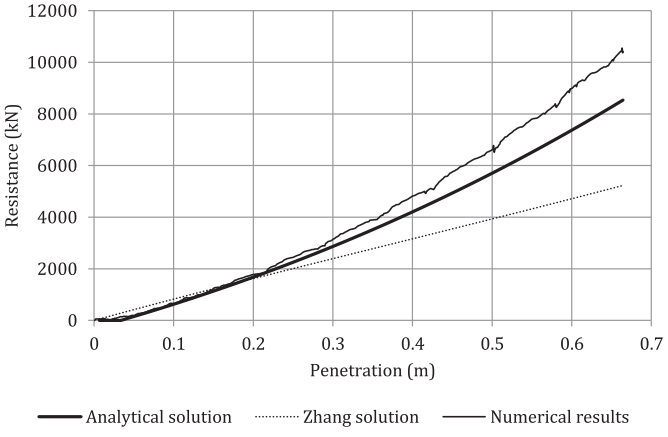

Fig. 8. Comparison between analytical and numerical results for $\alpha = 45°$.

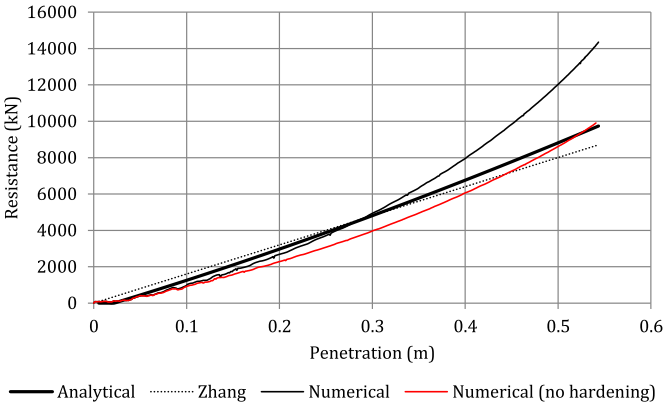

Fig. 9. Comparison between analytical and numerical results for $\alpha = 90°$.

be found by considering Eq. (1) and Fig. 1: if we denote by X_B the vertical position of point B along the X axis (see Fig. 1), it is easy to show that:

$$R_y = R_Y\sqrt{1-\frac{(X_P-X_B)^2}{R_X^2}}, \quad R_z = R_Z\left(1-\frac{(X_P-X_B)^2}{R_X^2}\right) \tag{15}$$

Consequently, substituting p and q by (15) in all the developments performed in Section 3 as well as in Appendix 1 leads to a closed-form expression of the resistance for solution 2. As a conclusion, a mathematical treatment is still needed for solution 1 only.

4.1. Definition of the displacements field

As mentioned here above, we will only focus on the first solution of Fig. 10. As a first step, let's consider the situation in the plane π_1 (see Fig. 11a), where the displacements are denoted by $W(x)$ and

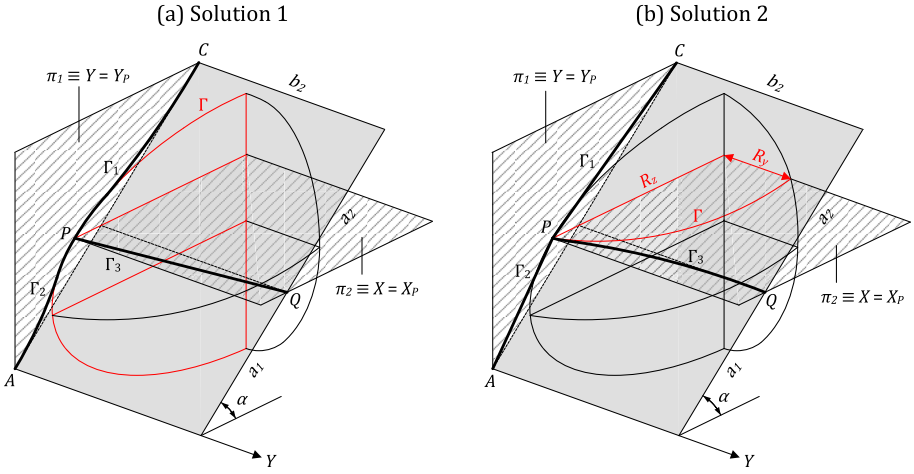

Fig. 10. Two different ways of defining the displacements field.

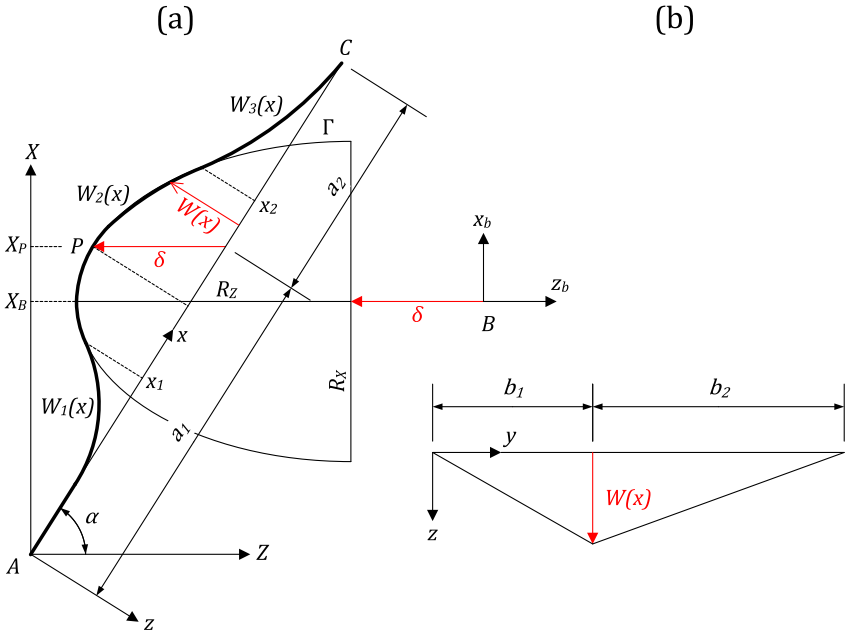

Fig. 11. (a) Displacements profile in the plane π_1; (b) displacements profile in the plane π_2.

defined in the direction perpendicular to the plate (i.e. along the z axis in Fig. 11a). By following the same procedure than in Section 3.1, $W(x)$ may be divided into three parts:

- For $x_1 \leq x \leq x_2$, the plate has to respect the shape of the bulb, which means that $W_2(x)$ has to be calculated in accordance with the mathematical expression of the parabola Γ (see Figs. 10a and 11a) corresponding to the intersection between the paraboloid $\mathbb{P}$ and the vertical plane π_1.
- For $0 \leq x < x_1$, $W_1(x)$ has to respect the support conditions $W_1 = 0$, $\partial W_1/\partial x = 0$ for $x = 0$ and the compatibility conditions $W_1 = W_2$, $\partial W_1/\partial x = \partial W_2/\partial x$ for $x = x_1$. This means that W_1 has to be a quadratic expression of x.
- For $x_2 < x \leq a$, $W_3(x)$ has to satisfy the support conditions $W_3 = 0$, $\partial W_3/\partial x = 0$ for $x = a$ and the compatibility conditions $W_3 = W_2$, $\partial W_3/\partial x = \partial W_2/\partial x$ for $x = x_2$. As a consequence, W_3 is also a quadratic expression of x.

This partition is in fact very similar to the one used for the case of an impact involving the stem, but one has to bear in mind that the displacements profile $W(x)$ is now defined in the direction perpendicular to the plate (i.e. along the z axis in Fig. 11a), while $W(y)$ was oriented along the global horizontal Z axis for a collision with the stem (see Section 3.1).

As we are working this time in the vertical plane π_1, we have to account for the inclination α of the plate, which means that the problem is mathematically more complex (this was not the case in Section 3.1 as the situation was analyzed in a horizontal plane). The mathematical developments leading to $W(x)$ are therefore more fastidious than those given by Eqs. (5)–(7). The derivation of a closed-form expression for $W(x)$ is therefore not presented here but is rather reported in Appendix 2.

At this stage, we will only present the final equations of $W(x)$. They may be derived as functions of the abscissas $x_{b,A}$ and $x_{b,C}$ of points A and C (see Fig. 11a) in the reference frame (x_b, y_b, z_b) fixed at point B (as mentioned in Section 2, this coordinate system is not moving with the bulb). It is important to realize that $x_{b,A}$ and $x_{b,C}$ may be evaluated by considering only the vertical position of the bulb X_B and other various geometrical data defining the collision scenario. Moreover, they are not independent, as

from Fig. 11a it is evident that $x_{b,C} = x_{b,A} + a\cot\alpha$. Following the developments detailed in Appendix 2, it may be shown that:

$$W_1(x) = \frac{1 + C_1 x\sin\alpha - \sqrt{1 + 2C_1 x\sin\alpha}}{C_1\cos\alpha} \quad \text{with} \quad 0 \le x < x_1 \tag{16}$$

$$W_2(x) = K_1 + x\tan\alpha - K_2\sqrt{K_3 + x\cos\alpha + \delta\cos^2\alpha} \quad \text{with} \quad x_1 \le x \le x_2 \tag{17}$$

$$W_3(x) = \frac{1 + C_2(x-a)\sin\alpha - \sqrt{1 + 2C_2(x-a)\sin\alpha}}{C_2\cos\alpha} \quad \text{with} \quad x_2 < x \le a \tag{18}$$

where the parameters C_1 to C_2 are functions of the indentation only. They are related to δ by Eq. (19), while the constant K_1 to K_3 are given by (20).

$$C_1 = \frac{4\delta\sin 2\alpha}{4R\delta - (2x_{b,A} - R\cot\alpha)^2}, \quad C_2 = \frac{4\delta\sin 2\alpha}{4R\delta - (2x_{b,C} - R\cot\alpha)^2} \quad \text{with} \quad R = \frac{R_X^2}{R_Z} \tag{19}$$

$$K_1 = \frac{R\tan\alpha + 2x_{b,A}}{2\cos\alpha}, \quad K_2 = \frac{\sqrt{R}}{\cos^2\alpha}, \quad K_3 = \frac{R}{4}\left(1 - \cot^2\alpha\right) + x_{b,A}\cot\alpha \tag{20}$$

The last step to have a complete definition of $W(x)$ is to precise the particular locations x_1 and x_2. These one may be found by imposing the compatibility conditions between $W_1(x)$, $W_2(x)$ and $W_3(x)$, as mentioned here over (additional information on the analytical derivation of x_1 and x_2 are reported in Appendix 2):

$$x_1 = \frac{4\delta\cos\alpha}{C_1}\,\frac{\delta\sin 2\alpha - 2x_{b,A} + R\cot\alpha}{(2x_{b,A} - R\cot\alpha)^2}, \quad x_2 = \frac{4\delta\cos\alpha}{C_2}\,\frac{\delta\sin 2\alpha - 2x_{b,C} + R\cot\alpha}{(2x_{b,C} - R\cot\alpha)^2} \tag{21}$$

where C_1, C_2 and e given by (19). $W(x)$ is entirely defined by Eqs. (16) and (21) and the displacement $w(x, y)$ of every point (x, y) of the plate is obtained by a linear interpolation of $W(x)$ along the y axis:

$$w(x,y) = W(x)f(y) \tag{22}$$

where the interpolation term $f(y)$ is simply varying linearly with y. Fig. 11b, shows that $f(y)$ has to be defined in two portions:

$$\begin{array}{ll} \text{For} & 0 \le y \le b_1: \quad f_1(y) = y/b_1 \\ \text{For} & b_1 < y \le b: \quad f_2(y) = (b-y)/b_2 \end{array} \tag{23}$$

which implies that $w(x,y)$ is not compatible at the junction $y = b_1$ as $\partial W/\partial y$ is not continuous. Once again, this problem may be solved by imposing a stationary hinge line at the particular location $y = b_1$. However, as the bending energy dissipated by this hinge is negligible in comparison with the membrane effects arising in the remaining parts of the plate, this phenomenon is disregarded and will not be mentioned anymore. The combination of $W(x)$ and $f(y)$ leading to $w(x, y)$ is summarized in Table 3.

Table 3
Combination of $f(y)$ and $W(x)$ to get the total field $w(x, y)$.

	$0 \le y \le b_1$	$b_1 < y \le b$
$0 \le x < x_1$	$W_1(x)\cdot f_1(y)$	$W_1(x)\cdot f_2(y)$
$x_1 \le x \le x_2$	$W_2(x)\cdot f_2(y)$	$W_2(x)\cdot f_2(y)$
$x_2 < x \le a$	$W_3(x)\cdot f_3(y)$	$W_3(x)\cdot f_2(y)$

It is clear from Eqs. (22) and (23) that $w(x, y)$ has the same direction than $W(x)$, i.e. perpendicular to the initial plane of the plate. As for the stem, this assumption implies that no friction is involved between the bulb and the impacted structure, which is a conservative hypothesis, as some energy would be dissipated by friction in reality.

4.2. Derivation of the resistance

As for the stem, the impact resistance is still derived by applying the upper-bound method. The displacements field $w(x, y)$ detailed in Section 4.1 is said to be kinematically admissible, as it is compatible (except at the junction $y = b_1$, but this problem is solved by imposing a plastic hinge at this particular location) and respects all the boundary conditions. The virtual velocities principle recalled in (9) may therefore be applied using $w(x, y)$ and the plate strip model leads finally to the collision resistance given by (14), i.e.:

$$F = \sigma_0 t_p \int_0^a dx \int_0^b \left(\frac{\partial w}{\partial x} \cdot \frac{\partial^2 w}{\partial x \partial \delta} + \frac{\partial w}{\partial x} \cdot \frac{\partial^2 w}{\partial \delta \partial x} \right) dy = \sum_{i=1}^{6} \left(\frac{\dot{E}_{x,i}}{\dot{\delta}} + \frac{\dot{E}_{y,i}}{\dot{\delta}} \right) \tag{24}$$

where $\dot{E}_{x,i}$ and $\dot{E}_{y,i}$ are the internal energy rates calculated for the six sub-areas dividing the plate according to Table 3. The procedure for deriving F is then strictly similar in the case of an impact by the stem or by the bulb, the only difference being the displacements field $w(x, y)$ to used to calculate the deformation rates (11). The expressions of the internal energy rate for an impact by the bulb are presented in Appendix 2.

So far, it is important to realize that two distinct formulae are available for the resistance. The first one F_1 is derived by respecting the exact shape of the bulb in the vertical plane π_1 (see solution 1 in Fig. 10a), while the second one F_2 is obtained when respecting the exact shape of the bulb in the horizontal plane π_2 (see solution 2 in Fig. 10b). Of course, the best would be to follow the bulb configuration in both horizontal and vertical directions, but unfortunately it is impossible to derive a closed-form solution for F in this case. Consequently, we have to choose between F_1 and F_2, as a unique value of F has to be selected for a given penetration δ.

An objective criterion for choosing between F_1 and F_2 may be simply defined by comparing the relative dimensions of the plate and of the bulb in the x and y dimensions. To do so, let us first consider the two extreme situations depicted in Fig. 12. The first one (Fig. 12a) is the case of a long plate in the y direction ($b \gg a$) impacted by a quite narrow bulb ($R_Y \ll R_X$). In such a case, it is clear that the deformations along the x axis are largely influenced by the shape of the bulb, while a linear approximation seems to be sufficient along the y axis. It is then important to choose a displacements field $w(x,$

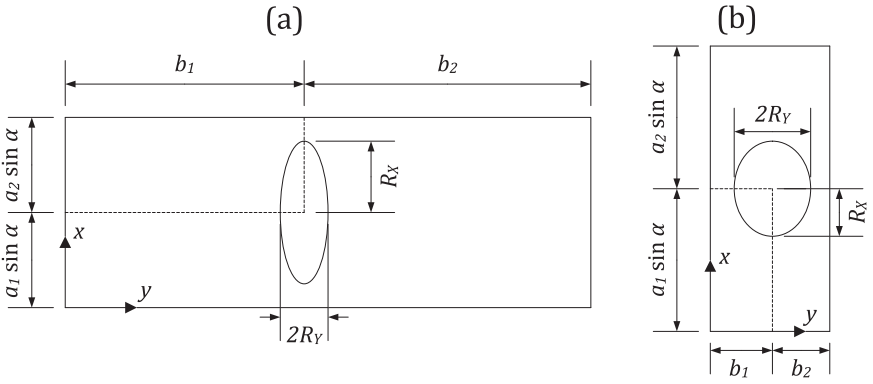

Fig. 12. Geometrical criteria for choosing between F_1 and F_2.

Table 4
Geometrical data used for numerical validations with LS-DYNA.

	Configuration 1			Configuration 2			Configuration 3		
Bulb	x Radius	R_X	2.5 m	x Radius	R_X	3 m	x radius	R_X	3 m
	y Radius	R_Y	2 m	y Radius	R_Y	1.5 m	y radius	R_Y	1.5 m
	z Radius	R_Z	3 m	z Radius	R_Z	3 m	z radius	R_Z	3 m
Plate	x Dimension	a	5 m	x Dimension	a	4 m	x dimension	a	6 m
	y Dimension	b	4 m	y Dimension	b	6 m	y dimension	b	4 m
	Thickness	t_p	0.01 m	Thickness	t_p	0.01 m	Thickness	t_p	0.01 m

y) that respects the exact shape of the bulb in the vertical plane π_1, so the resistance F_1 given by solution 1 has to be kept. On the contrary, for the situation depicted in Fig. 12b, it is clear that solution 2 provides a more realistic approach for deriving the resistance and F_2 has to be retained. Finally, a geometrical criterion for choosing between F_1 and F_2 may be expressed as:

$$\begin{array}{llll} \text{if}: & \max(R_X/a_1; R_X/a_2) \rangle \max(R_Y/b_1; R_Y/b_2) & \text{then solution 1 is kept}: & F = F_1 \\ \text{if}: & \max(R_X/a_1; R_X/a_2) \langle \max(R_Y/b_1; R_Y/b_2) & \text{then solution 2 is kept}: & F = F_2 \end{array} \tag{25}$$

4.3. Numerical validation

In Section 3.3, we gave a quite succinct numerical validation for the case of an impact involving the stem. This was motivated by the fact that other comparisons for this collision scenario have already been published in Ref. [11]. However, as an impact involving the bulb has not been treated in an earlier publication, we decided to give more details in Section 3.3. Regarding the simulations performed using LS-DYNA, the mechanical properties of the materiel are still those presented in Table 2 but this time three different geometrical situations (listed in Table 4) are considered. The first one is used to check if the analytical approximation of the resistance is valid while considering various inclinations, so different values of the angle α are tested for configuration 1. Configurations 2 and 3 aim to check if the criterion (25) is realistic or not. Therefore, the ratio b/R_Y is quite large for configuration 2, while the ratio a/R_X is predominant for configuration 3. In both cases, only the results obtained for $\alpha = 60°$ are presented. It is worth noting that the aim of this section is only to provide a numerical validation of the analytical developments detailed above. As a consequence, the plate dimensions chosen in Table 4 are not necessarily realistic regarding a classical ship architecture.

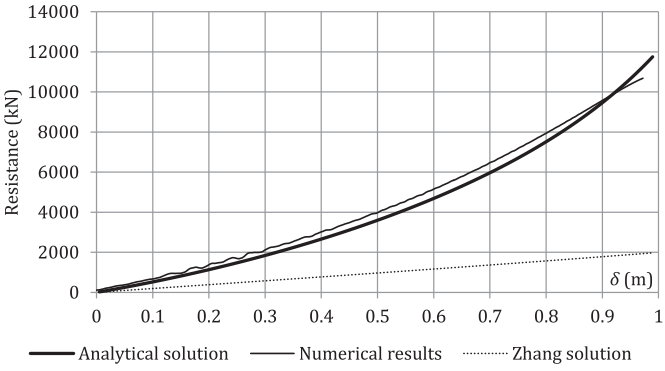

Fig. 13. Configuration 1: comparison between analytical and numerical results for $\alpha = 45°$.

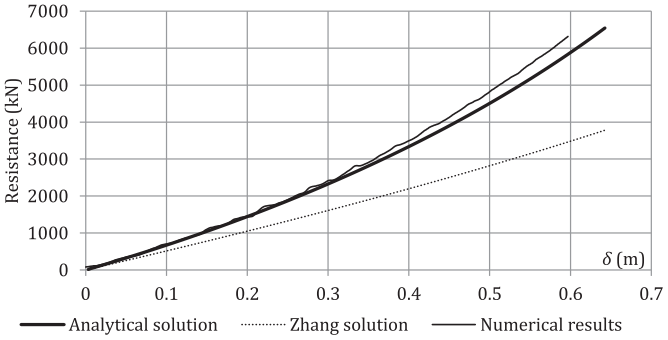

Fig. 14. Configuration 1: comparison between analytical and numerical results for $\alpha = 60°$.

The results obtained for configuration 1 are plotted in Figs. 13–16. They show that the concordance of the present simplified analytical procedure with numerical simulations is satisfactory for all the values of α. The resistance predicted by Zhang [7] is also plotted on these figures (the corresponding formula is given by Eq. (57) in Appendix 1). As it can be seen, the discrepancy between the curves obtained with LS-DYNA and with Zhang solution is quite important, especially for the small values of α as Zhang solution is proportional to $\sin^2 \alpha$. Figs. 13–16 show that assimilating the collision process to a punctual impact comes to drastically underestimate the resistance F, in particular for small values of α. It is therefore of prior importance to account for the shape of the striking bulb as it may have a strong influence on the deformations, and consequently also on the amount of energy dissipated by the inclined plate.

It is worth noting that the previous conclusions are specific to the case of a striking bulb. Indeed, as depicted in Figs. 8 or 9 for the stem, there is a better agreement between Zhang formula and LS-DYNA. This simply means that a collision involving the stem may be idealized in a better way by a punctual impact, which is probably due to the fact that the stem has a sharper form than the bulb. Consequently, one has always to be careful before using a punctual approximation, whose validity is directly related to the shape of the impactor. Representing the collision process with a point load may result in an overestimation of F when δ is small and in an underestimation of F with increasing values of δ.

Figs. 17 and 18 present the results obtained in case of a larger plate than the one considered previously. For configuration 2, the long and small sides of the plate are respectively oriented along y and x direction. According to (25), the deformations along the x axis are more influenced by the shape of the

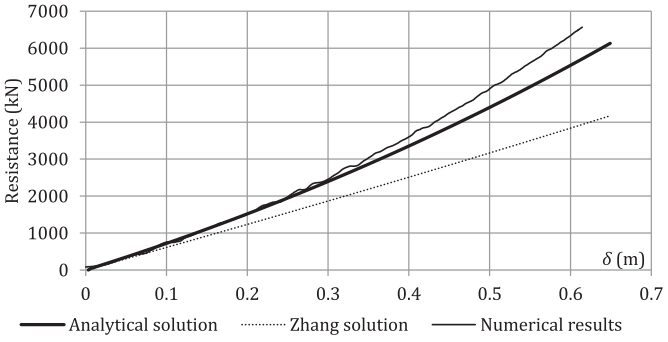

Fig. 15. Configuration 1: comparison between analytical and numerical results for $\alpha = 75°$.

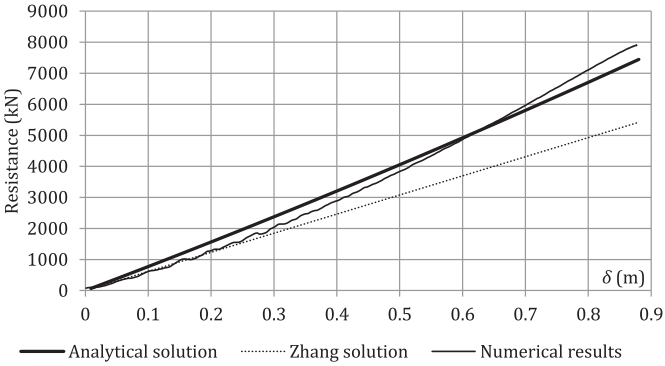

Fig. 16. Configuration 1: comparison between analytical and numerical results for $\alpha = 90°$.

bulb, so solution 2 has to be selected. Fig. 17 shows that the analytical procedure for evaluating F in this case is satisfactory. For configuration 3, the plate is positioned the other way round, i.e. that its long and small sides are respectively oriented along x and y direction. In this case, the resistance F has to be evaluated with solution 1. Doing so provides a quite satisfactory estimation of F, as shown by Fig. 18. Consequently, it seems that (25) is sufficient for choosing between the two different ways illustrated in Fig. 10.

5. Impact on a full scale ship

In a recent communication [11], Buldgen et al. investigated the collision of a rigid bow impacting a ship having an inclined side shell. In this study, the struck vessel is modeled only by one of its section bounded by two transverse bulkheads (Fig. 19a). It is supposed to be resting against a quay, which prohibits any sway and roll motion. To point out the importance of accounting for the inclination of the plating, the analysis is performed for $\alpha = 80°$ and $\alpha = 45°$. More information about the finite elements modeling parameters for the struck and striking vessels are detailed in Section 4 of Ref. [11].

The simulations of the collision process are performed with LS-DYNA for the two different values of α. In each case, the parameters used for defining the material properties of the struck elements are those given in Table 2, while the striking bow (Fig. 19b) is defined as a rigid body. In this study, the

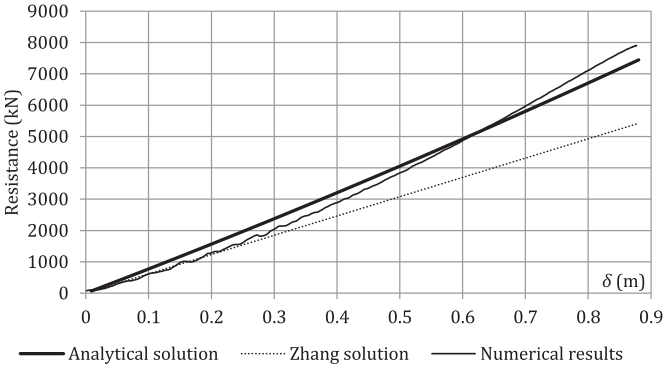

Fig. 17. Configuration 2: comparison between analytical and numerical results for $\alpha = 60°$.

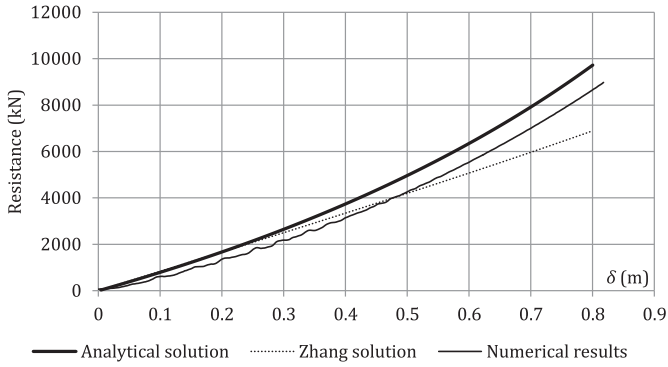

Fig. 18. Configuration 3: comparison between analytical and numerical results for $\alpha = 60°$.

5. Impact on a full scale ship

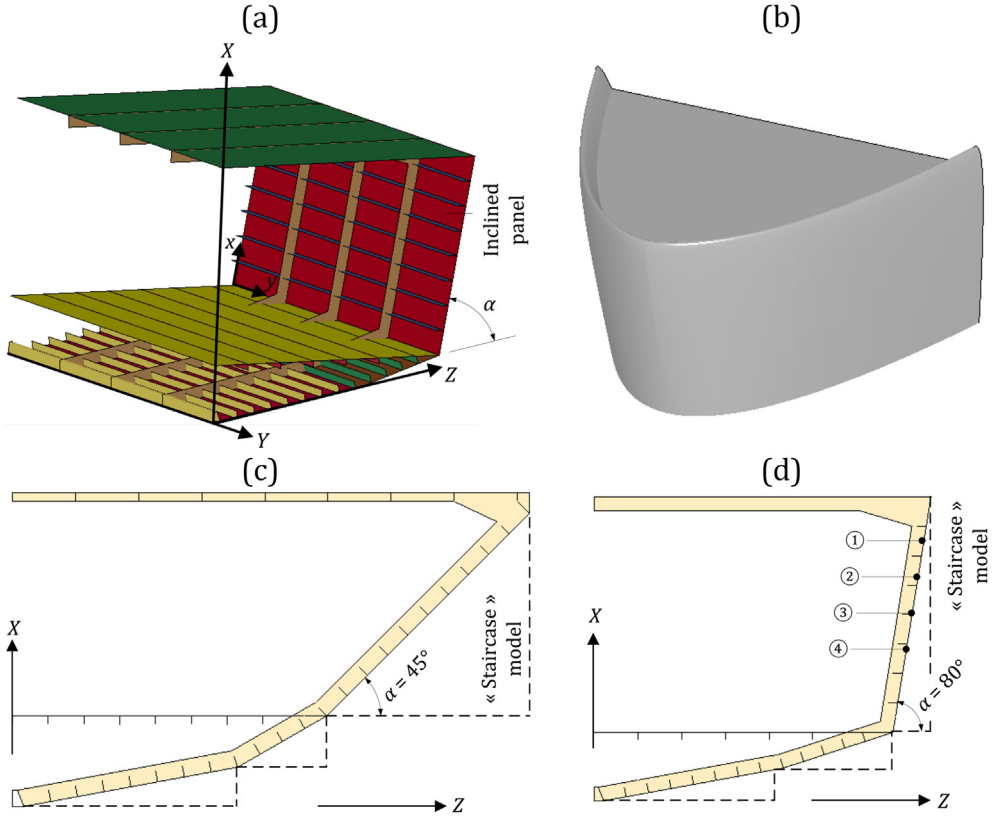

Fig. 19. (a) Section of the ship; (b) striking bow; (c) struck vessel for $\alpha = 45°$; (d) struck vessel for $\alpha = 80°$.

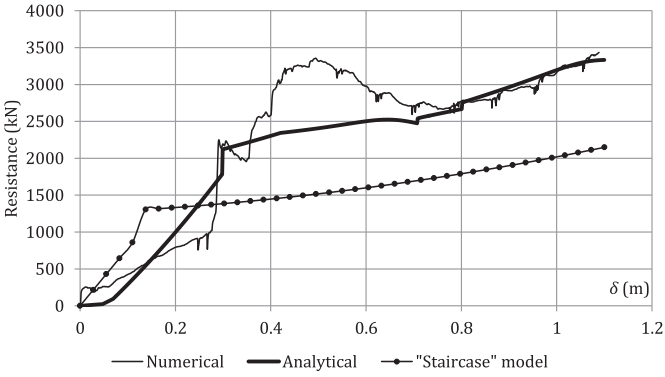

Fig. 20. Comparison between numerical and analytical results for $\alpha = 80°$.

numerical curves giving $F(\delta)$ are compared to those derived by the super-elements methods (see Figs. 20 and 21 that are extracted from Ref. [11] without modification). In this approach, the inclined ship side is modeled by using the new super-element developed here above. The transverse webs are treated as separated components, which are assumed to be folded during the collision process. Their contributions to the collision resistance is simply evaluated by using the classical formula developed by Simonsen and recalled by Eq. (57) in Appendix 1. On the other hand, the longitudinal stiffeners are supposed to be only subjected to membrane extension. Therefore, they may be smeared by increasing fictitiously the original thickness t_p of the super-element. Thus, for a panel reinforced by n stiffeners of cross section A_i (with $1 \leq i \leq n$) parallel to the y axis (Fig. 19), the equivalent thickness t_{eq} is given by:

$$t_{eq} = t_p + \sum_{i=1}^{n} \frac{A_i}{b} \tag{26}$$

where b is the extension of the plate along the y direction. In order to illustrate the contribution of the present new inclined plate component, the struck ship is also decomposed in a staircase model (see Fig. 19c and d), as it could already be achieved with the only horizontal and vertical super-elements available so far.

As depicted in Figs. 20 and 21, the agreement between the results provided by LS-DYNA and the super-elements method integrating the new inclined components is found to be satisfactory. On the

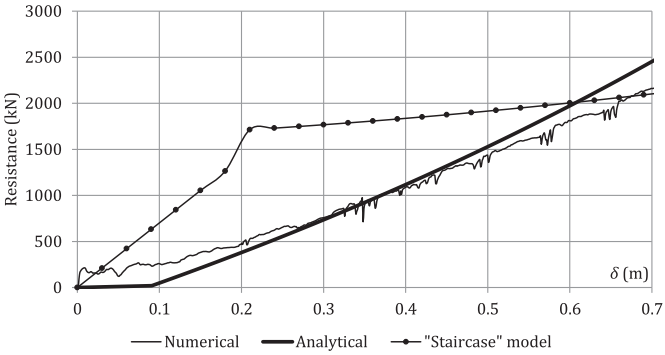

Fig. 21. Comparison between numerical and analytical results for $\alpha = 45$.

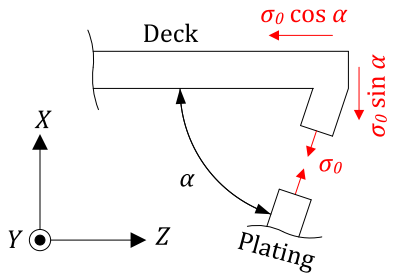

Fig. 22. Stress division at the junction between the inclined side shell and the uppermost deck.

contrary, this not the case for the "staircase" model, for which the discrepancy is much larger. This shows the importance of accounting for the inclination of the plating.

However, during this study, Buldgen et al. [11] noticed that the collision resistance tends to be overestimate at the beginning of the indentation. This is particularly visible for $0.15 \leq \delta \leq 0.3$ in Fig. 20 and may be explained as follows. If we refer to the plate strip model developed by Wierzbicki [10], the inclined panel of Fig. 19a may be seen as a set of plastic fibers oriented along the local axes x and y. Consequently, the tensile yield stress σ_0 acting on each fiber parallel to x has to be supported by the uppermost deck, as shown in Fig. 22. This means that the deck is submitted to compression because of the horizontal component $\sigma_0 \cos\alpha$, but also to bending by the action of $\sigma_0 \sin\alpha$.

Under an impact, for increasing values of the indentation, the inclination of the plating is varying with δ from α to $\alpha - \Delta\alpha$ (Fig. 23a), which causes the vertical component of σ_0 to decrease from $\sigma_0 \sin\alpha$ to $\sigma_0 \sin(\alpha - \Delta\alpha)$. As a consequence, if the deck is perfectly rigid, the bending action $m_d = L_d \sigma_0 \sin(\alpha - \Delta\alpha)$ is progressively vanishing for larger values of δ (Fig. 23a). On the contrary, if the deck is flexible enough, the tensile stress σ_0 produces a growing second-order vertical displacement Δ_X (Fig. 23b) that leads to the following bending action on the deck:

$$m_d = (L_d - \Delta_Z)\sigma_0 \sin(\alpha - \Delta\alpha) + \Delta_X \sigma_0 \cos(\alpha - \Delta\alpha) \tag{27}$$

It is difficult to predict from (27) if m_d is increasing or decreasing with δ. However, this last formula points out that the bending effects in the deck do not necessarily tend to stabilize as the penetration is getting larger, even if the vertical component of σ_0 is decreasing.

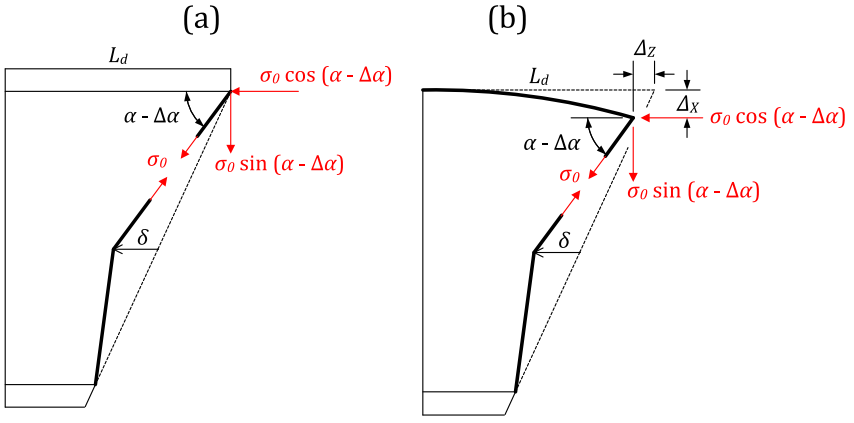

Fig. 23. (a) Stress distribution in case of a (a) rigid deck; (b) flexible deck.

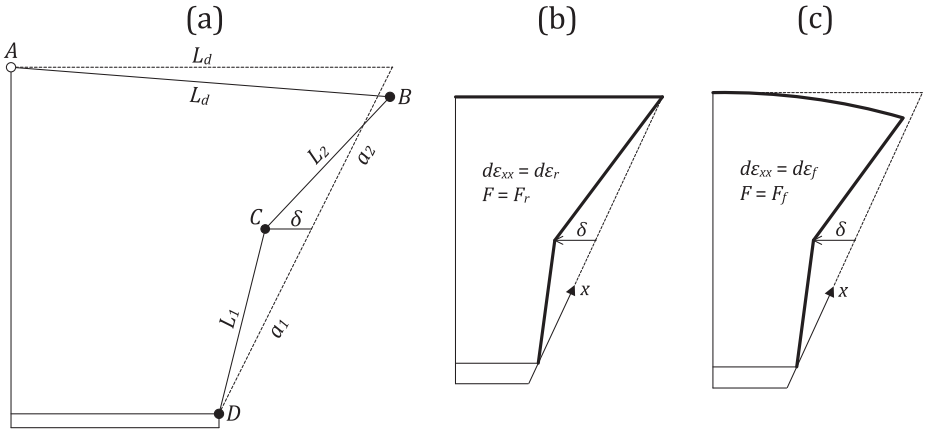

Fig. 24. (a) Mechanism for a very flexible deck; Deformation pattern for a (a) rigid or (b) flexible deck.

From all the previous considerations, it is worth remembering that the deck is submitted to bending because of the membrane effects appearing in the impacted inclined plating. The resistance provided by the plate therefore lower than the one theoretically predicted in the present paper. Indeed, in formula (14) and (12) giving the resistance F, the deformation rates $\dot{\varepsilon}_{xx}$ are calculated under the assumption of non-moving plate supports, which is actually the case if the deck is rigid enough (Fig. 24b). Let us denote by $\dot{\varepsilon}_r$ and F_r the values of $\dot{\varepsilon}_{xx}$ and F derived under this hypothesis. For a flexible deck (Fig. 24c), the supports are not fixed anymore, and one may calculate other values $\dot{\varepsilon}_f$ and F_f for $\dot{\varepsilon}_{xx}$ and F in this case. Applying (14), we have:

$$F_r = \frac{\sigma_0 t_p}{\dot{\delta}} \int_0^a dx \int_0^b (\dot{\varepsilon}_r + \dot{\varepsilon}_{yy}) dy, \quad F_f = \frac{\sigma_0 t_p}{\dot{\delta}} \int_0^a dx \int_0^b \left(\dot{\varepsilon}_f + \dot{\varepsilon}_{yy}\right) dy \tag{28}$$

Comparing Fig. 24b and c, it may be intuitively accepted that $\dot{\varepsilon}_f < \dot{\varepsilon}_r$, so that $F_f < F_r$. In other words, the resistance provided by the plate in case of a flexible deck is less than the one obtained for a rigid one. If we go one step further, a very flexible deck may be seen to be simply supported (see point A in Fig. 24a) and completely free to rotate as a rigid body. Under this hypothesis, it is possible for the plating to move like a mechanism through the action of three plastic hinges located at points B, C and D in Fig. 24a. In such a case, $L_1 + L_2 = a_1 + a_2$ and no membrane effects are induced in the fibers oriented along the x axis. Such an assumption leads to the conclusion that the membrane deformation rate is

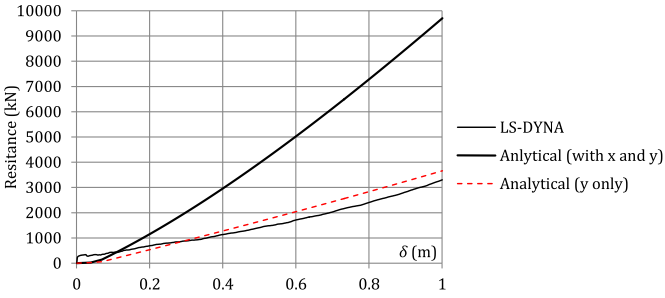

Fig. 25. Resistance for collision scenario ①.

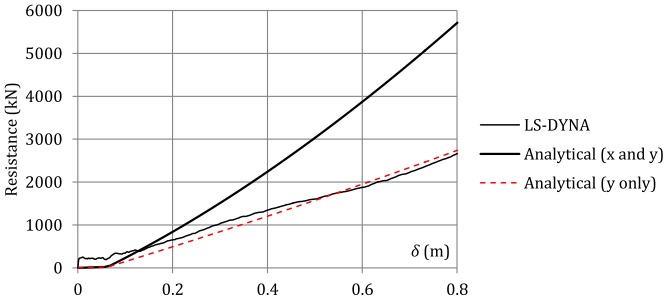

Fig. 26. Resistance for collision scenario ②.

simply $\dot{\varepsilon}_{xx} = 0$. The plastic dissipation is only confined in the hinges, which is practically negligible for quite thin plates. As a consequence, applying (14), we get:

$$F = \frac{\sigma_0 t_p}{\dot{\delta}} \int_0^a \mathrm{d}x \int_0^b \dot{\varepsilon}_{yy}\, \mathrm{d}y \tag{29}$$

which shows that the plate resistance is only coming from the fibers parallel to the y axis. As shearing is not taken into account, (29) provides a more conservative approach than evaluating F by considering also shear strain energy.

In order to study the importance of accounting for the flexibility of the deck, we can consider the struck ship with $\alpha = 80°$ (Fig. 19d) and perform four different collision simulations. For each of them, the impact point is successively shifted from ① to ④ in Fig. 19d. The bending effects in the deck are then expected to be progressively reduced as the contact location is taken away from the uppermost deck. The results for each collision scenario are plotted in Figs. 25–28. In order to focus only on the sections presenting the largest discrepancy, the simulations have been stopped before any subsequent contact between the striking vessel and the lower deck.

The curve called "Analytical (with x and y)" corresponds to the resistance calculated analytically with Eq. (12), i.e. by accounting for the contribution of both the x- and y-fibers. The curve denoted by "Analytical (y only)" is obtained by using Eq. (29), i.e. by considering only the contribution coming from the y-fibers.

From Figs. 25–28, it is clear that the coupling between the decks and the present inclined plate has to be taken into account. If this is not the case, the analytical approach may lead to an overestimation of the collision resistance. As detailed previously, a solution to this problem is to neglect the membrane energy dissipated by the fibers parallel to the x axis. A better agreement with the LS-DYNA results is

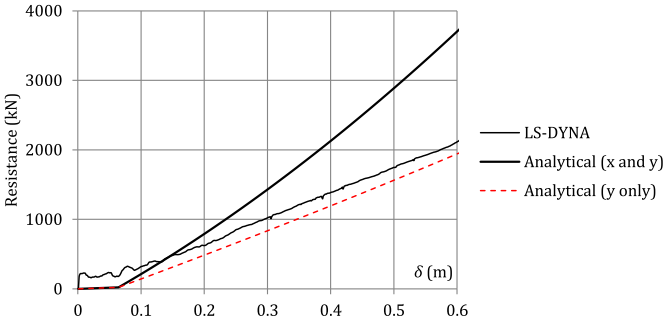

Fig. 27. Resistance for collision scenario ③.

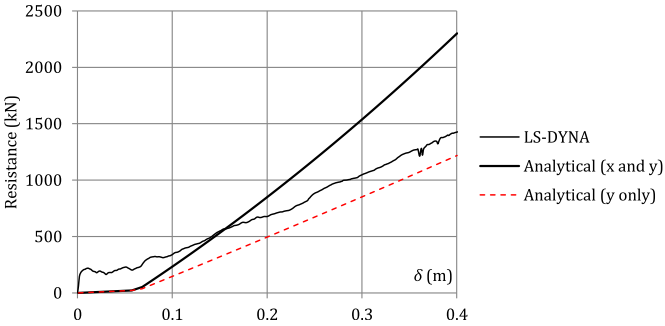

Fig. 28. Resistance for collision scenario ④.

then found, as it can be seen in Figs. 25–28. Nevertheless, this approach is not totally satisfactory because the problem is much more related to the applied methodology. Indeed, the super-elements method is based on the assumption that the various components are decoupled and only activated in case of a direct contact with the bow, which is not the case for the present situation.

6. Conclusion

In this paper, we propose closed-form expressions allowing for a rapid prediction of the resistance opposed by an inclined plate during a collision. This work is achieved by considering that the plate is impacted by the stem or by the bulb of a striking vessel. The formulae are derived by accounting for the particular shape of the impactor. By comparing them with other results already available in the literature and derived under the assumption of a punctual impact, it is shown that the real profile of the colliding bow has to be considered to get a realistic approximation of the resistance.

The developments are first validated individually, by comparing the resistance derived analytically with numerical results obtained by simulating collisions on isolated inclined plates. The accordance is found to be satisfactory for both the bulb and the stem. It is also shown that the present developments are convenient as well for treating collisions between two ships. This global validation is performed by recalling results of full scale ship collisions already mentioned by the authors [11]. Finally, a particular attention is devoted to study the influence of having a flexible deck. It is pointed out that the hypothesis of working with uncoupled super-elements is not realistic for some cases. Further research is therefore necessary to modify this method in order to consider coupling when developing analytical approaches.

It transpires from the validation process that the present simplified analytical treatment of ship collisions tends to lead to crushing forces that are lower than those obtained through numerical calculations. Nevertheless, as the analytical solution is based on the upper-bound method applied to a given specific mode of deformation, the numerical solution may be expected to be stiffer than the analytical one, which is actually not the case (see Figs. 8, 14 and 20 for example). However, one has to bear in mind that:

- the analytical prediction does not account for strain hardening, while a non-zero tangent modulus is used in the numerical simulations.
- the influence of bending occurring in the uppermost deck is not considered while evaluating the membrane resistance of the new inclined super-element.

For these two main reasons, the super-elements methods leads to softer results than the finite elements methods. Nevertheless, one can say that the method provides a quick estimation of the resistance having a quite reasonable agreement with numerical results.

The new inclined plate super-element presented in this paper is currently integrated in a global analysis tool (called SHARP) that is based on the super-element methods [13]. As soon as this work is

achieved, it will be also possible to simulate offshore collisions between two sailing vessels, and not only an impact occurring on a ship resting against a quay.

Appendix 1. Analytical derivation of the energy rate for an impact by the stem

In this appendix, we will give some more details on the way to derive the analytical resistance of an inclined plate impacted by the stem of a ship. As detailed in Section 3.1 and summarized in Table 1, $w(x, y)$ is defined differently over the eight sub-areas dividing the plate. Let us adopt the numbering convention depicted in Fig. 29, where each region ① to ⑧ is limited by the intersecting dotted lines.

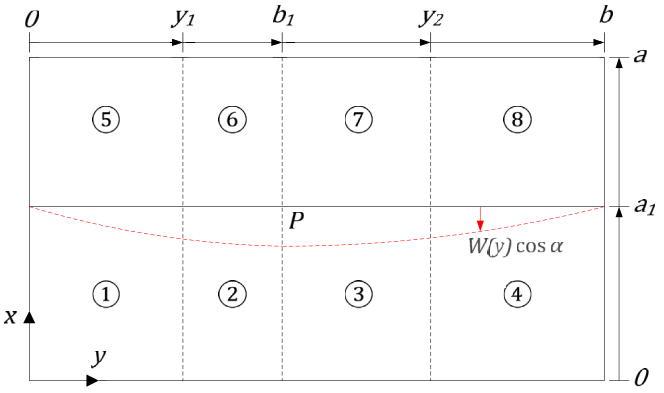

Fig. 29. Subdivision of the impacted plate.

During the impact, each of these regions may be characterized by an individual internal energy rate $\dot{E}_i$ (with $1 \le i \le 8$) and the total energy rate for the plate $\dot{E}_{\text{int}}$ is simply obtained by summation:

$$\dot{E}_{\text{int}} = \sum_{i=1}^{8} \dot{E}_i = \sum_{i=1}^{8} \left(\dot{E}_{x,i} + \dot{E}_{y,i} \right) \tag{30}$$

Starting from the definitions of $w(x,y)$ given in Section 3.1 and applying Eqs. (11) and (12), it is possible to derive the different contributions E_i for the eight sub-areas. However, providing an exhaustive derivation of each $\dot{E}_i$ may therefore be quite fastidious and redundant. For this reason, we will limit our developments to the regions ① and ② limited by $0 \le y \le b_1$ and $0 \le x \le a_1 - W(y)\cos\alpha$ (see Fig. 5 and Table 1) and simply present the final analytical expressions of $\dot{E}_i$ for the other parts. These results have already been presented in a less detailed manner in another paper [11]. So let us first consider the area ① defined by $(x, y) \in [0; a_1 - W_1(y)\cos\alpha] \times [0; y_1]$, where the displacements field according to Table 1 is given by $w(x, y) = f_1(x) \cdot W_1(y)$. Taking into account the relations (6), (7) and (8), we get the following expression:

$$w(x,y) = W_1(y) \frac{x \sin\alpha}{a_1 - W_1(y)\cos\alpha}, \quad W_1(y) = \delta \frac{y^2}{b_1 y_1}, \quad y_1 = b_1 - \frac{q^2 \delta}{p b_1} \tag{31}$$

Applying the definitions given in (11), the deformation rates (and other useful relations as well) are found to be:

$$\dot{\varepsilon}_{xx} = \frac{a_1 \sin^2\alpha}{(a_1 - W_1(y)\cos\alpha)^3} W_1(y) \frac{\partial W_1}{\partial \delta} \dot{\delta} \tag{32}$$

$$\dot{\varepsilon}_{yy} = \frac{a_1^2 x^2 \sin^2\alpha}{(a_1 - W_1(y)\cos\alpha)^5}\frac{\partial W_1}{\partial y}\left((a_1 - W_1(y)\cos\alpha)\frac{\partial^2 W_1}{\partial y\partial\delta} + 2\frac{\partial W_1}{\partial y}\frac{\partial W_1}{\partial\delta}\cos\alpha\right)\dot{\delta} \tag{33}$$

$$\text{with :} \quad \frac{\partial W_1}{\partial y} = 2\delta\frac{y}{b_1 y_1}, \quad \frac{\partial W_1}{\partial\delta} = \frac{y^2}{y_1^2}, \quad \frac{\partial^2 W_1}{\partial y\partial\delta} = \frac{2y}{y_1^2} \tag{34}$$

Substituting expressions (32) and (33) in (12) gives the internal energy rate characterizing the area under consideration. For this first area, we get:

$$\dot{E}_{x,1} = \int_0^{y_1} \frac{\sigma_0 t_p \dot{\delta} a_1 \sin^2\alpha}{(a_1 - W_1(y)\cos\alpha)^2} W_1(y)\frac{\partial W_1}{\partial\delta}\mathrm{d}y \tag{35}$$

$$\dot{E}_{y,1} = \int_0^{y_1} \frac{\sigma_0 t_p \dot{\delta} a_1^2 \sin^2\alpha}{3(a_1 - W_1(y)\cos\alpha)^2}\frac{\partial W_1}{\partial y}\left((a_1 - W_1(y)\cos\alpha)\frac{\partial^2 W_1}{\partial y\partial\delta} + 2\frac{\partial W_1}{\partial y}\frac{\partial W_1}{\partial\delta}\cos\alpha\right)\mathrm{d}y \tag{36}$$

Using relations (31) and (34), we finally get the closed-form expressions for internal energy rates that are similar to those already exposed in Ref. [11]:

$$\dot{E}_{x,1} = \frac{y_1 \sin^2\alpha}{2(1-f_1)\cos\alpha} + \frac{3a_1 b_1 \sin^2\alpha}{2\delta\cos^2\alpha}\left(1 - \frac{\operatorname{arctanh}\left(\sqrt{f_1}\right)}{\sqrt{f_1}}\right), \quad f_1 = \frac{y_1\delta\cos\alpha}{a_1 b_1} \tag{37}$$

$$\dot{E}_{y,1} = \frac{8a_1^2\sin^2\alpha}{3y_1\cos\alpha}\left(1 - \frac{\operatorname{arctanh}\left(\sqrt{f_1}\right)}{\sqrt{f_1}}\right) + \frac{4\delta a_1 \sin^2\alpha}{3b_1(1-f_1)} \tag{38}$$

Let us now consider area ② defined by $(x, y) \in [0;\ a_1 - W_2(y)\cos\alpha] \times [y_1;\ b_1]$. The corresponding displacements are given by (see Table 1) $w(x, y) = f_1(x)\cdot W_2(y)$. According to (5) and (8), one may write:

$$w(x,y) = W_2(y)\frac{x\sin\alpha}{a_1 - W_2(y)\cos\alpha}, \quad W_2(y) = \delta - \frac{p(y-b_1)^2}{q^2} \tag{39}$$

It is clear that $\dot{\varepsilon}_{xx}$ and $\dot{\varepsilon}_{yy}$ are still given by (32) and (33), but $W_1(y)$ is replaced by $W_2(y)$ and the derived terms become:

$$\frac{\partial W_2}{\partial y} = -2p\frac{y-b_1}{q^2}, \quad \frac{\partial W_2}{\partial\delta} = 1, \quad \frac{\partial^2 W_2}{\partial y\partial\delta} = 0 \tag{40}$$

Introducing these results into Eqs. (35) and (36), the internal energy rates associated to the deformation of the fibers oriented along x and y are respectively given by:

$$\dot{E}_{x,2} = \int_{y_1}^{b_1} \frac{\sigma_0 t_p \dot{\delta} a_1 \sin^2\alpha}{(a_1 - W_2(y)\cos\alpha)^2} W_2(y)\mathrm{d}y \tag{41}$$

$$\dot{E}_{y,2} = \int_{y_1}^{b_1} \frac{2\sigma_0 t_p \dot{\delta} a_1^2 \sin^2\alpha\cos\alpha}{3(a_1 - W_2(y)\cos\alpha)^2}\left(\frac{\partial W_2}{\partial y}\right)^2 \mathrm{d}y \tag{42}$$

The expressions of $W_2(y)$ and $\partial W_2/\partial y$ given in (39) and (40) may be used to perform the two previous integrations, which leads to the same results than those already exposed in Ref. [11]:

$$\dot{E}_{x,2} = \frac{a_1^2 \sin^2\alpha}{2(a_1-\delta\cos\alpha)^2\cos\alpha}\left(\frac{2\delta\cos\alpha - a_1}{a_1}\,\frac{b_1-y_1}{f_2}\arctan(f_2) + \frac{b_1-y_1}{1+f_2^2}\right) \tag{43}$$

$$\dot{E}_{y,2} = \frac{4p}{3q^2}\,\frac{a_1^2\sin^2\alpha}{a_1-\delta\cos\alpha}\left(\frac{b_1-y_1}{f_2}\arctan(f_2) - \frac{b_1-y_1}{1+f_2^2}\right), \quad f_2 = \frac{b_1-y_1}{q}\sqrt{\frac{p\cos\alpha}{a_1-\delta\cos\alpha}} \tag{44}$$

A similar procedure is followed for the sub-areas ③ to ⑧ to derive the closed-form expressions of the internal energy rates. This leads to the equations exposed hereafter, which are also mentioned in Ref. [11]:

- For sub-area ③ defined by $(x, y) \in [0;\, a_1 - W_2(y)\cos\alpha] \times [b_1;\, y_2]$:

$$\dot{E}_{x,3} = \frac{a_1^2 \sin^2\alpha}{2(a_1-\delta\cos\alpha)^2\cos\alpha}\left(\frac{2\delta\cos\alpha - a_1}{a_1}\,\frac{y_2-b_1}{f_3}\arctan(f_3) + \frac{y_2-b_1}{1+f_3^2}\right) \tag{45}$$

$$\dot{E}_{y,3} = \frac{4p}{3q^2}\,\frac{a_1^2\sin^2\alpha}{a_1-\delta\cos\alpha}\left(\frac{y_2-b_1}{f_3}\arctan(f_3) - \frac{y_2-b_1}{1+f_3^2}\right), \quad f_3 = \frac{y_2-b_1}{q}\sqrt{\frac{p\cos\alpha}{a_1-\delta\cos\alpha}} \tag{46}$$

- For sub-area ④ defined by $(x, y) \in [0;\, a_1 - W_3(y)\cos\alpha] \times [y_2;\, b]$:

$$\dot{E}_{x,4} = \frac{(b-y_2)\sin^2\alpha}{2(1-f_4)\cos\alpha} + \frac{3a_1b_2\sin^2\alpha}{2\delta\cos^2\alpha}\left(1 - \frac{\operatorname{arctanh}\left(\sqrt{f_4}\right)}{\sqrt{f_4}}\right), \quad f_4 = \frac{(b-y_2)\delta\cos\alpha}{a_1b_2} \tag{47}$$

$$\dot{E}_{y,4} = \frac{8a_1^2\sin^2\alpha}{3(b-y_2)\cos\alpha}\left(1 - \frac{\arctan h\left(\sqrt{f_4}\right)}{\sqrt{f_4}}\right) + \frac{4\delta a_1\sin^2\alpha}{3b_2(1-f_4)} \tag{48}$$

- For sub-area ⑤ defined by $(x, y) \in [a_1 - W_1(y)\cos\alpha;\, a] \times [0;\, y_1]$:

$$\dot{E}_{x,5} = \frac{3a_2b_1\sin^2\alpha}{2\delta\cos^2\alpha}\left(1 - \frac{\arctan\left(\sqrt{f_5}\right)}{\sqrt{f_5}}\right) - \frac{y_1\sin^2\alpha}{2(1+f_5)\cos\alpha}, \quad f_5 = \frac{y_1\delta\cos\alpha}{a_2b_1} \tag{49}$$

$$\dot{E}_{y,5} = \frac{16a_2^2\sin^2\alpha}{3y_1\cos\alpha}\left(1 - \frac{\arctan\left(\sqrt{f_5}\right)}{\sqrt{f_5}}\right) - \frac{4\delta a_2\sin^2\alpha}{3b_1(1+f_5)} \tag{50}$$

- For sub-area ⑥ defined by $(x, y) \in [a_1 - W_2(y)\cos\alpha; a] \times [y_1; b_1]$:

$$\dot{E}_{x,6} = \frac{a_2^2 \sin^2\alpha}{2(a_2 + \delta\cos\alpha)^2 \cos\alpha}\left(\frac{2\delta\cos\alpha + a_2}{a_2}\frac{b_1 - y_1}{f_6}\operatorname{arctanh}(f_6) - \frac{b_1 - y_1}{1 - f_6^2}\right) \tag{51}$$

$$\dot{E}_{y,6} = \frac{4p}{3q^2}\,\frac{a_2^2 \sin^2\alpha}{a_2 + \delta\cos\alpha}\left(\frac{b_1 - y_1}{f_6}\operatorname{arctanh}(f_6) - \frac{b_1 - y_1}{1 + f_6^2}\right), \quad f_6 = \frac{b_1 - y_1}{q}\sqrt{\frac{p\cos\alpha}{a_2 + \delta\cos\alpha}} \tag{52}$$

- For sub-area ⑦ defined by $(x, y) \in [a_1 - W_2(y)\cos\alpha; a] \times [y_1; b_1]$:

$$\dot{E}_{x,7} = \frac{a_2^2 \sin^2\alpha}{2(a_2 + \delta\cos\alpha)^2 \cos\alpha}\left(\frac{2\delta\cos\alpha + a_2}{a_2}\frac{y_2 - b_1}{f_7}\operatorname{arctanh}(f_7) - \frac{y_2 - b_1}{1 - f_7^2}\right) \tag{53}$$

$$\dot{E}_{y,7} = \frac{4p}{3q^2}\,\frac{a_2^2 \sin^2\alpha}{a_2 + \delta\cos\alpha}\left(\frac{y_2 - b_1}{f_7}\operatorname{arctanh}(f_6) - \frac{y_2 - b_1}{1 + f_7^2}\right), \quad f_7 = \frac{y_2 - b_1}{q}\sqrt{\frac{p\cos\alpha}{a_2 + \delta\cos\alpha}} \tag{54}$$

- For sub-area ⑧ defined by $(x, y) \in [a_1 - W_1(y)\cos\alpha; a] \times [0; y_1]$:

$$\dot{E}_{x,8} = \frac{3a_2 b_2 \sin^2\alpha}{2\delta\cos^2\alpha}\left(1 - \frac{\arctan\left(\sqrt{f_8}\right)}{\sqrt{f_8}}\right) - \frac{(b - y_2)\sin^2\alpha}{2(1 + f_8)\cos\alpha}, \quad f_8 = \frac{(b - y_2)\delta\cos\alpha}{a_2 b_2} \tag{55}$$

$$\dot{E}_{y,8} = \frac{16a_2^2 \sin^2\alpha}{3(b - y_2)\cos\alpha}\left(1 - \frac{\arctan\left(\sqrt{f_8}\right)}{\sqrt{f_8}}\right) - \frac{4\delta a_2 \sin^2\alpha}{3b_2(1 + f_8)} \tag{56}$$

As a final step, the total resistance provided by the plate is simply obtained by applying the virtual work principle detailed in (14), where $\dot{E}_{x,i}$ and $\dot{E}_{y,i}$ are given by Eqs. (35), (36) and (43) to (56) for $1 \le i \le 8$. As a matter of comparison, it is worth noting that Zhang [7] also found an analytical solution for the problem considered in the present paper. However, the procedure exposed in Ref. [7] considers a punctual impact and therefore does not account for the shape of the striking vessel. According to this author, one may evaluate the resistance F by the expression:

$$F = \frac{2\sigma_0 t_p}{3\sqrt{3}}\,\delta(b_1 + b_2)\left(\frac{a_1 + a_2}{a_1 a_2} + \frac{a_1}{(a_1 - \delta\cos\alpha)^2} + \frac{a_2}{(a_2 + \delta\cos\alpha)^2}\right)\sin^2\alpha \tag{57}$$

Closed-form expressions are also available for the particular case of an impact occurring on a horizontal plate (i.e. for $\alpha = 0°$). Amongst others, Simonsen [12] provides the following formula for this particular case:

$$F = \frac{1.56\sigma_0 t_p^{5/3}(b_1+b_2)}{(b_1 b_2)^{1/3}} + \frac{0.518\sigma_0 t_p^{4/3}(b_1+b_2)}{(b_1 b_2)^{2/3}}\left(1+\frac{\delta}{1.51(b_1 b_2 t_p)^{1/3}}\right)\delta \tag{58}$$

Appendix 2. Analytical derivation of the energy rate for an impact by the bulb

As the second solution represented in Fig. 10b is formally similar to the case of an impact by the stem, this appendix is only devoted to study the first solution of Fig. 10a, where the displacements field $w(x, y)$ is defined to account for the true shape of the bulb in the plane π_1. So we will only deal with the derivation of F_1 in the present section.

As summarized in Table 3, $w(x, y)$ is different over the six sub-areas dividing the plate. These ones may be numbered as depicted in Fig. 30, where the intersection between the plane π_1 and the plane (x, y) of the plate is materialized by the vertical dotted line located in $y = b_1$ (which is also a plastic hinge line). Note that in this appendix, only the study of the three first regions is presented and the results are simply extrapolated for the regions 4–6 (b_1 is then replaced by $b_2 = b - b_1$).

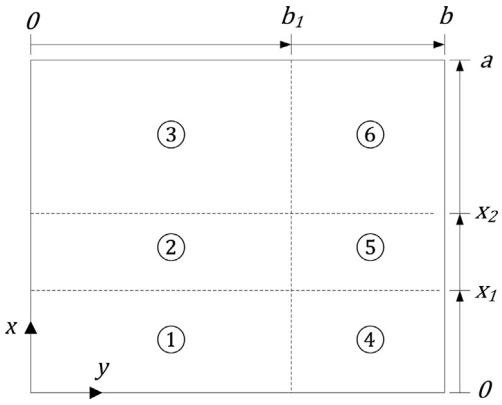

Fig. 30. Subdivision of the impacted plate.

The first step to get the resistance F is to determine the analytical expression of $w(x, y)$. As detailed in Section 4.1, $w(x, y)$ is given by $W(x)f(y)$, where $f(y)$ is simply a linear function y/b_1. The mathematical equation of $W(x)$ is more complicated to establish. For this reason, it is probably easier to work initially in the reference frame (x_b, z_b) of the bulb than directly in the axes (x, z) associated to the plate. To do so, let us start by decomposing the displacements profile into the three parts Γ_1, Γ_2 and Γ_3 depicted in Fig. 31. On area ②, Γ_2 has to stick to the curve Γ describing the shape of the striking bulb into the particular plane $\pi_1 \equiv y_b = 0$. The expression of Γ (and consequently of Γ_2) is found by substituting $y_b = 0$ in Eq. (1), which leads to:

$$\frac{x_b^2}{R_X^2} = \frac{z_b + R_Z + \delta}{R_Z} \Leftrightarrow \Gamma_2 \equiv z_b = R_Z\left(\frac{x_b^2}{R_X^2} - 1\right) - \delta \tag{59}$$

Once the curve Γ_2 is mathematically described, the analytical expressions for both curves Γ_1 and Γ_3 may be written:

$$\Gamma_1 \equiv z_b = \alpha_1 x_b^2 + \beta_1 x_b + \gamma_1, \quad \Gamma_3 \equiv z_b = \alpha_2 x_b^2 + \beta_2 x_b + \gamma_2 \tag{60}$$

where the parameters $\alpha_1, \alpha_2, \beta_1, \beta_2, \gamma_1, \gamma_2$ have still to be determined. This may be achieved by writing the compatibility conditions between Γ_1 and Γ_2 or between Γ_3 and Γ_2. First of all, curve Γ_1 has to respect the following conditions:

- At the junction between areas ① and ② denoted by point 1 in Fig. 31, the displacements and rotations have to coincide, i.e.:

$$\Gamma_1 = \Gamma_2 \Leftrightarrow R_Z\left(\frac{x_{b,1}^2}{R_X^2} - 1\right) - \delta = \alpha_1 x_{b,1}^2 + \beta_1 x_{b,1} + \gamma_1 \tag{61}$$

$$\frac{\partial \Gamma_1}{\partial x_b} = \frac{\partial \Gamma_2}{\partial x_b} \Leftrightarrow \frac{2R_Z}{R_X^2} x_{b,1} = 2\alpha_1 x_{b,1} + \beta_1 \tag{62}$$

- Along the supported edge denoted by point A in Fig. 31, the relative displacements and rotations have to be set to zero, i.e.:

$$A \in \Gamma_1 \Leftrightarrow \alpha_1 x_{b,A}^2 + \beta_1 x_{b,A} + \gamma_1 = z_{b,A} \tag{63}$$

$$\frac{\partial \Gamma_1}{\partial x_b} = \cot\alpha \Leftrightarrow \cot\alpha = 2\alpha_1 x_{b,A} + \beta_1 \tag{64}$$

where, as already mentioned in Section 4.1, $x_{b,A}$ and $z_{b,A}$ are the coordinates of point A in the reference frame (x_b, z_b). Once again, it is important to realize both parameters are directly related to the relative position of the bulb with respect to the plate. As a consequence, $x_{b,A}$ and $z_{b,A}$ are perfectly known if the collision scenario is correctly defined.

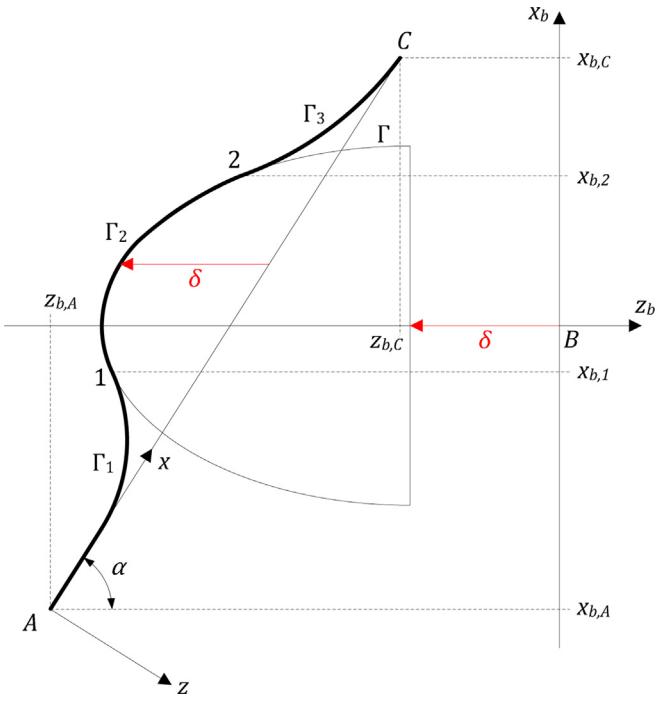

Fig. 31. Displacements profile in the plane π_1.

Finally, we get the four equations (Eqs. (61)–(64)) to fix only the three unknowns α_1, β_1 and γ_1. Nevertheless, one has to bear in mind that the position $x_{b,1}$ present in Eq. (61) is in fact an additional unknown, as the junction between areas ① and ② has not been defined so far. Solving this system of equations leads to the following results:

$$\Gamma_1 \equiv z_b = \frac{2C_1}{\sin 2\alpha}(x_b - x_{b,A})^2 + (x_b - x_{b,A})\cot\alpha + z_{b,A} \tag{65}$$

$$x_{b,1} = R\frac{2(\delta + R_Z + z_{b,A}) - x_{b,A}\cot\alpha}{2x_{b,A} - R\cot\alpha} \tag{66}$$

where C_1 and R are given by (19). The same procedure may be followed to derive the analytical expression of the last curve Γ_3. By expressing the compatibility at point 2 and imposing the support conditions at point C in Fig. 31, the following expressions are obtained:

$$\Gamma_3 \equiv z_b = \frac{2C_2}{\sin 2\alpha}(x_b - x_{b,C})^2 + (x_b - x_{b,C})\cot\alpha + z_{b,C} \tag{67}$$

$$x_{b,2} = R\frac{2(\delta + R_Z + z_{b,C}) - x_{b,C}\cot\alpha}{2x_{b,C} - R\cot\alpha} \tag{68}$$

where C_2 is also given in (19). Finally, the locations $z_{b,1}$ and $z_{b,2}$ of points 1 and 2 along the z_b axis may be found by expressing that these points also belongs to the curve Γ defining the bulb. As a consequence, their coordinates have to verify (59), i.e.:

$$z_{b,1} = R_Z\left(\frac{x_{b,1}^2}{R_X^2} - 1\right) - \delta, \quad z_{b,2} = R_Z\left(\frac{x_{b,2}^2}{R_X^2} - 1\right) - \delta \tag{69}$$

in which $x_{b,1}$ and $x_{b,2}$ are respectively obtained by (66) and (68). The deformation profile is now entirely defined in the axes (x_b, z_b) by the mathematical expressions of Γ_1, Γ_2, Γ_3 given by (59), (65), (67) and by the coordinates of the junction points 1 and 2 in (66), (68), (69). Before deriving the expressions of $W_1(x)$, $W_2(x)$ and $W_3(x)$, coordinates of the junction points 1 and 2 are switch from the reference frame (x_b, z_b) of the bulb to the axes (x, z) associated to the plate. To do so, the following formulae are used:

$$x = (x_b - x_{b,A})\sin\alpha + (z_b - z_{b,A})\cos\alpha, \quad z = -(x_b - x_{b,A})\cos\alpha + (z_b - z_{b,A})\sin\alpha \tag{70}$$

Eqs. (66), (68) and (69) are then introduced in (70), which leads to the expressions of x_1 and x_2 given by (21). Similarly, using (70) in (59), (65), (67) and expressing z as a function of x leads to the analytical expressions of $W_1(x)$, $W_2(x)$ and $W_3(x)$ given by (16), (17) and (18). Once the displacements field $w(x, y)$ has been derived over the six sub-areas depicted in Fig. 30, it is possible to establish an analytical expression for F with help of formula (24). Therefore, the energy rates $\dot{E}_{x,i}$ and $\dot{E}_{y,i}$ have first to be evaluated for the sub-areas ① to ⑥ shown in Fig. 30. In this optic, let us first start by calculating the following useful derivatives:

$$\begin{aligned}
&\frac{\partial W_1}{\partial x} = \left(1 - \frac{1}{\sqrt{1+2C_1 x\sin\alpha}}\right)\tan\alpha, \quad \frac{\partial W_1}{\partial \delta} = \frac{1}{C_1^2\sin\alpha}\left(\frac{1+C_1 x\sin\alpha}{\sqrt{1+2C_1 x\sin\alpha}} - 1\right)\frac{\partial C_1}{\partial \delta}\\
&\frac{\partial^2 W_1}{\partial x\partial\delta} = \frac{x\tan\alpha\sin\alpha}{(1+2C_1 x\sin\alpha)^{3/2}}\frac{\partial C_1}{\partial\delta}, \quad \frac{\partial W_2}{\partial x} = \tan\alpha - \frac{K_2\cos\alpha}{2\sqrt{K_3 + \delta\cos^2\alpha + x\cos\alpha}}\\
&\frac{\partial W_2}{\partial\delta} = -\frac{K_2\cos^2\alpha}{2\sqrt{K_3 + \delta\cos^2\alpha + x\cos\alpha}}, \quad \frac{\partial^2 W_2}{\partial x\partial\delta} = \frac{K_2\cos^3\alpha}{4(K_3 + \delta\cos^2\alpha + x\cos\alpha)^{3/2}}
\end{aligned} \tag{71}$$

where $\partial C_1/\partial\delta$ may be found by deriving (19) with respect to δ. The derivatives $\partial W_3/\partial x$, $\partial W_3/\partial\delta$ and $\partial^2 W_3/\partial x\partial\delta$ are not given by (71) but they are simply given by replacing C_1 by C_2 and x by $a-x$ in the corresponding formulae for $W_1(x)$. Once all the required mathematical results are available, the energy rates for regions ① to ③ can be calculated and extrapolated to the regions ④ to ⑥. This is achieved hereafter:

- For sub-area ① defined by $(x, y) \in [0; x_1] \times [0; b_1]$:

$$\dot{E}_{x,1} = \sigma_0 t_p \int_0^{b_1} dy \int_0^{x_1} \dot{\varepsilon}_{xx}\, dx = \sigma_0 t_p \dot{\delta} \int_0^{b_1} f_1^2(y) dy \int_0^{x_1} \frac{\partial W_1}{\partial x} \cdot \frac{\partial^2 W_1}{\partial x \partial \delta}\, dx \tag{72}$$

$$\Leftrightarrow \dot{E}_{x,1} = \frac{b_1 \sigma_0 t_p}{3C_1^2} \frac{\sin\alpha}{\cos^2\alpha} \frac{\partial C_1}{\partial \delta} \left(\sqrt{g_1(\delta)} - 1 - \frac{g_2(\delta)}{\sqrt{g_1(\delta)}} + \frac{g_2(\delta)}{2g_1(\delta)} - \frac{1}{2} \ln \sqrt{g_1(\delta)} \right) \dot{\delta} \tag{73}$$

$$\dot{E}_{y,1} = \sigma_0 t_p \int_0^{b_1} dy \int_0^{x_1} \dot{\varepsilon}_{yy}\, dx = \sigma_0 t_p \dot{\delta} \int_0^{b_1} \left(\frac{\partial f_1}{\partial y} \right)^2 dy \int_0^{x_1} \frac{\partial W_1}{\partial x} \cdot W_1(x)\, dx \tag{74}$$

$$\Leftrightarrow \dot{E}_{y,1} = \frac{\sigma_0 t_p}{5b_1} \frac{\sqrt{g_1(\delta)}\left(g_2^2(\delta) + 6g_2(\delta) + 4\right) - 4 - 5g_2(\delta)(g_2(\delta) + 2)}{C_1^4 \sin\alpha \cos^2\alpha} \dot{\delta} \tag{75}$$

$$\text{with :} \quad g_1(\delta) = 1 + 2g_2(\delta) \quad g_2(\delta) = C_1 x_1 \sin\alpha \tag{76}$$

- For sub-area ② defined by $(x, y) \in [x_1; x_2] \times [0; b_1]$:

$$\dot{E}_{x,2} = \sigma_0 t_p \int_0^{b_1} dy \int_{x_1}^{x_2} \dot{\varepsilon}_{xx}\, dx = \sigma_0 t_p \dot{\delta} \int_0^{b_1} f_1^2(y) dy \int_{x_1}^{x_2} \frac{\partial W_2}{\partial x} \cdot \frac{\partial^2 W_2}{\partial x \partial \delta}\, dx \tag{77}$$

$$\Leftrightarrow \dot{E}_{x,2} = \frac{b_1 \sigma_0 t_p}{24} K_2 \cos^2\alpha \left(\frac{K_2 \cos\alpha - 4\tan\alpha\sqrt{g_3(\delta)}}{g_3(\delta)} - \frac{K_2 \cos\alpha - 4\tan\alpha\sqrt{g_4(\delta)}}{g_4(\delta)} \right) \dot{\delta} \tag{78}$$

$$\dot{E}_{y,2} = \sigma_0 t_p \int_0^{b_1} dy \int_{x_1}^{x_2} \dot{\varepsilon}_{yy}\, dx = \sigma_0 t_p \dot{\delta} \int_0^{b_1} \left(\frac{\partial f_1}{\partial y} \right)^2 dy \int_{x_1}^{x_2} \frac{\partial W_2}{\partial x} W_2(x) dx \tag{79}$$

$$\Leftrightarrow \dot{E}_{y,2} = \sigma_0 t_p \frac{K_2 \cos\alpha}{b_2} \left(\frac{K_2 \cos\alpha}{2} (x_2 - x_1) + g_6(\delta)\sqrt{g_4(\delta)} - g_5(\delta)\sqrt{g_3(\delta)} \right) \dot{\delta} \tag{80}$$

$$\text{with :} \quad \begin{array}{ll} g_3(\delta) = K_3 + \delta\cos^2\alpha + x_2\cos\alpha, & g_5(\delta) = K_1 - \frac{\tan\alpha}{3}\left(2\frac{K_3+\delta\sin^2\alpha}{\cos\alpha} - x_2\right) \\ g_4(\delta) = K_3 + \delta\cos^2\alpha + x_1\cos\alpha, & g_6(\delta) = K_1 - \frac{\tan\alpha}{3}\left(2\frac{K_3+\delta\sin^2\alpha}{\cos\alpha} - x_1\right) \end{array} \tag{81}$$

- For sub-area ③ defined by $(x, y) \in [x_2; a] \times [0; b_1]$: the mathematical equation of $\dot{E}_{x,3}$ and $\dot{E}_{y,3}$ may be found simply by substituting $C_1 \equiv C_2$ and $x_1 \equiv x_2 - a$ in (73), (75) and (76). The signs of the so obtained expressions have then to be changed to get the final form of the rates $\dot{E}_{x,3}$ and $\dot{E}_{y,3}$.

Concerning the three remaining regions ④ to ⑥, it is clear that the corresponding energy rates are simply given by substituting $b_1 \equiv b_2$ in the equations derived here over for the areas ① to ③. Finally, introducing all the above results of $\dot{E}_{x,i}$ and $\dot{E}_{y,i}$ in (24) leads to the desired closed-form expression of F.

References

[1] Minorsky VU. An analysis of ship collisions with reference to nuclear power plants. J Ship Res 1959;3:1–4.
[2] Pedersen PT. Review and application of ship collision and grounding analysis procedures. Mar Struct 2010;23:241–62.
[3] Ueda Y, Rashed SMH. The idealized structural unit method and its application to deep girder structures. Comput Struct 1984;18:277–93.
[4] Lützen M, Simonsen BC, Pedersen PT. Rapid prediction of damage to struck and striking vessels in a collision even, International conference of ship structures for the new millennium: supporting quality in shipbuilding, Arlington; 2000.
[5] Le Sourne H. A ship collision analysis program based on super-element method coupled with large rotational ship movement analysis tool. International conference on collision and grounding of ships, ICCGS-2007; 2007. p. 131–8.
[6] Jones N. Structural impact. Cambridge: Cambridge University Press; 1997.
[7] Zhang SM. The mechanics of ship collisions. PhD. thesis. Department of Naval Architecture and Offshore Engineering, Technical University of Denmark; 1999.
[8] Wang G. Some recent studies on plastic behavior of plates subjected to large impact loads. J Offshore Mech Arctic Eng 2002;124:125–31.
[9] Wang G, Ohtsubo H. Deformation of ship plate subjected to very large load. J Offshore Mech Arctic Eng 1997;119:173–80.
[10] Wierzbicki T, Simonsen BC. Rupture analysis of oil tankers in a side collision: global structural model of bow indentation into ship side. In: US coast guard 1995. Washington: Oil Pollution Research Grants Publications; 1997.
[11] Buldgen L, Le Sourne H, Rigo P. A new super-element for estimating the collision resistance of an inclined ship side. Proceedings of the fourth international conference on marine structures – Marstruct 2013, Espoo, Finland; 25–27 March 2013.
[12] Simonsen BC, Ocakli H. Experiments and theory on deck girder crushing. Thin-walled Struct 1999;34:195–216.
[13] Le Sourne H, Besnard N, Cheylan C, Buannic N. A ship collision analysis program based on upper bound solutions and coupled with a large rotational ship movement analysis tool. J Appl Math 2012. http://dx.doi.org/10.1155/2012/375686.